Los Alamos NATIONAL LABORATORY EST.1943

LA-UR-19-28502 (Accepted Manuscript)

Understanding the eco-geomorphologic feedback of coastal marsh under sea level rise: vegetation dynamic representations, processes interaction, and parametric sensitivity

Zhang, Yu
Rowland, Joel C.
Xu, Chonggang
Wolfram, Phillip Justin Jr.
Svyatsky, Daniil
Moulton, John David
Marani, Marco
D'Alpaos, Andrea
Cao, Zhendong
Pasqualini, Donatella

Provided by the author(s) and the Los Alamos National Laboratory (2020-11-04).

To be published in: Journal of Geophysical Research: Earth Surface

DOI to publisher's version: 10.1029/2020JF005729

Permalink to record: http://permalink.lanl.gov/object/view?what=info:lanl-repo/lareport/LA-UR-19-28502

Disclaimer:
Los Alamos National Laboratory, an affirmative action/equal opportunity employer, is operated by Triad National Security, LLC for the National Nuclear Security Administration of U.S. Department of Energy under contract 89233218CNA000001. By approving this article, the publisher recognizes that the U.S. Government retains nonexclusive, royalty-free license to publish or reproduce the published form of this contribution, or to allow others to do so, for U.S. Government purposes. Los Alamos National Laboratory requests that the publisher identify this article as work performed under the auspices of the U.S. Department of Energy. Los Alamos National Laboratory strongly supports academic freedom and a researcher's right to publish; as an institution, however, the Laboratory does not endorse the viewpoint of a publication or guarantee its technical correctness.

RESEARCH LIBRARY

Check for updates

Accepted Article

Understanding the eco-geomorphologic feedback of coastal marsh under sea level rise: vegetation dynamic representations, processes interaction, and parametric sensitivity

Yu Zhang[1], Joel C. Rowland[1], Chonggang Xu[1], Phillip J. Wolfram[2], Daniil Svyatsky[2], J. David Moulton[2], Zhendong Cao[2], Marco Marani[3,4,5], Andrea D'Alpaos[6], and Donatella Pasqualini[7]

[1]Earth and Environmental Sciences Division, Los Alamos National Laboratory, Los Alamos, NM, USA.

[2]Theoretical Division, Los Alamos National Laboratory, Los Alamos, NM, USA.

[3]Division of Earth and Ocean Sciences, Duke University, Durham, NC, USA.

[4]Department of Civil and Environmental Engineering, Duke University, Durham, NC, USA.

[5]Dipartimento di Ingegneria Civile, Edile ed Ambientale, Universita' degli studi di Padova, Padova, Italy.

[6]Department of Geosciences, University of Padova, Via Gradenigo 6, 35131 Padova, Italy

[7]Analytics, Intelligence & Technology Division, Los Alamos National Laboratory, Los Alamos, NM, USA.

Corresponding author: Yu Zhang (yuzhang@lanl.gov)

This article has been accepted for publication and undergone full peer review but has not been through the copyediting, typesetting, pagination and proofreading process, which may lead to differences between this version and the Version of Record. Please cite this article as doi: 10.1029/2020JF005729.

This article is protected by copyright. All rights reserved.

Accepted Article

Key Points:

- Marsh platform relief increases with sea level rise rate
- The nonlinear *Spartina* scheme is the most resilient scheme, and the linear *Spartina* scheme predicts the lowest unvegetated□vegetated ratio
- Models become more sensitive to vegetation parameters for increasing sea level rise rates

This article is protected by copyright. All rights reserved.

Accepted Article

Abstract

A growing number of coastal eco-geomorphologic modeling studies have been conducted to understand coastal marsh evolution under sea-level rise (SLR). Although these models quantify marsh topographic change as a function of sedimentation and erosion, their representations of vegetation dynamics that control organic sedimentation differ. How vegetation dynamic schemes contribute to simulation outcomes is not well quantified. Additionally, the sensitivity of modeling outcomes to parameter selection in the available formulations has not been rigorously tested to date, especially under the influence of an accelerating SLR. In this paper, we used a coastal eco-geomorphologic model with different vegetation dynamic schemes to investigate the eco-geomorphologic feedbacks of coastal marshes and parametric sensitivity under SLR scenarios. We found that marsh platform relief increased with sea level rise rate. The simulations with different vegetation schemes exhibited different spatial-temporal variations in elevation and biomass. The nonlinear *Spartina* scheme presented the most resilient prediction with generally the highest marsh accretion and vegetation biomass, and the least elevation relief under SLR. But the linear *Spartina* scheme predicts the lowest unvegetated□vegetated ratio. We also found that vegetation-related parameters and sediment diffusivity, which were not well measured or discussed in previous studies, were identified as some of the most critical parameters. Additionally, the model sensitivity to vegetation-related parameters increased with SLR rates. The identified most sensitive parameters may inform how to appropriately choose modeling representations of key processes and parameters for different coastal marsh landscapes under SLR, and demonstrate the importance of future field measurements of these key parameters.

Keywords: Landscape evolution, Eco-geomorphologic model, Coastal marsh, Sea level rise, Accretion, Vulnerability

This article is protected by copyright. All rights reserved.

Accepted Article

1 Introduction

Coastal marshes are unique landscapes that connect terrestrial and aquatic systems and provide important ecosystem services, such as sustaining wildlife habitats, protecting shorelines, attenuating floods, storing carbon, and filtering contaminants (Barbier et al., 2011; Costanza et al., 1997; Fagherazzi, 2014; FitzGerald & Hughes, 2019; Roulet, 1990; Tiner, 2013). Intensified climate change, especially accelerating sea level rise (SLR), storm surges and associated extreme sea levels, and reduced sediment transport to the coastal zone threaten the stability of coastal marsh ecosystems (Cahoon & Guntenspergen, 2010; Ratliff et al., 2015; Scavia et al., 2002; Yousefi Lalimi et al., 2020). The vertical accretion rate for coastal marsh surfaces is the difference between the sedimentation rate and the surface erosion rate and is controlled by complex eco-geomorphologic interactions at multiple scales. To survive, the vertical accretion rate must at least keep pace with the rate of relative SLR (i.e. SLR + subsidence rate, Burkett & Kusler, 2000; Day et al., 2008; Kirwan et al., 2010; Marani et al., 2007; Reed, 1995). Therefore, investigating how eco-geomorphologic processes respond to SLR is a prerequisite for understanding the sustainability and resilience of coastal ecosystem structure and functions to SLR.

The term eco-geomorphology, which highlights the interactions between landscapes and ecosystems, can be traced back to the concept of bio-geomorphology in the pioneering study by *Viles* [1988], who explicitly considered the interactive roles of biota and geomorphology in landscape development. Later, a more comprehensive description of the linkage between coastal hydrology, vegetation dynamics, and geomorphology was gradually established by early-stage modeling studies (Allen, 2000; D'Alpaos et al., 2007; French, 1993; Kirwan & Murray, 2007; Marani et al., 2007; Morris et al., 2002; Mudd et al., 2004, 2009; Randerson, 1979; van Wijnen

This article is protected by copyright. All rights reserved.

Accepted Article

& Bakker, 2001). The diagram presented in Figure 1 includes the key components that control the eco-geomorphologic feedbacks in coastal ecosystems and provides a conceptual framework for model development and analysis. Here, the state and dynamics of a hydro-eco-geomorphic system is described in terms of three variables (marsh elevation, vegetation biomass, and ocean drivers including saltwater intrusion, tide, wave, storm surge, and sea level rise (SLR)) and three sediment fluxes (inorganic sediment deposition, organic soil production, and erosion) (Allen, 2000; Marani et al., 2007, 2010). The elevation of marshland with respect to the mean sea level, which may change over time, is controlled by accretion through inorganic sediment deposition, organic soil production, and erosion, as well as by land subsidence (soil compaction and sediment decomposition) and SLR. Tidal currents, waves, and storm surges directly drive sediment dynamics via sediment deposition and erosion. Changes in tidal range affect the depth, frequency, and duration of flooding of marsh plants, and therefore changes soil salinity, oxygen and sulfide availability affecting plant growth (Silvestri & Marani, 2004). Vegetation plays a critical role in decreasing water velocity and dissipating wave energy, thereby reducing sediment erosion and increasing deposition (Carus et al., 2016; Ghisalberti & Nepf, 2005; Moller et al., 2014; Nepf, 1999; Yang et al., 2012). Vegetation also contributes to sedimentation by directly trapping suspended sediment and by producing organic matter in the subsurface (Mudd et al., 2004). Changes in marsh elevation produce changes in water levels on marshland, thereby affecting marsh plant development (Morris et al., 2002; Mudd et al., 2004).

[Approximated location of Figure 1]

Using this conceptual framework, a number of mathematical models have been developed to describe and understand the evolution of coastal marshes under SLR (e.g., Allen, 2000; Best et al., 2018; Da Lio et al., 2013; D'Alpaos et al., 2007; Duvall et al., 2019; French,

This article is protected by copyright. All rights reserved.

Accepted Article

1993, 2006; Kirwan et al., 2010; Kirwan, Temmerman, et al., 2016; Kirwan, Walters, et al., 2016; Kirwan & Murray, 2007; Kirwan & Temmerman, 2009; Langston et al., 2020; Marani et al., 2007, 2013; Mariotti & Fagherazzi, 2010; Morris & Bowden, 1986; Mudd et al., 2009; Rogers et al., 2012; Schile et al., 2014; Schuerch et al., 2018; Stralberg et al., 2011; Thorne et al., 2018; van Wijnen & Bakker, 2001). Although these models vary in complexity, all provide insights into coastal marsh vulnerability under SLR, especially for understanding whether the accretion rate of marshland can keep pace with the rate of SLR.

For their representation of vegetation-related processes, some modeling studies assumed static vegetation with a constant influence of vegetation on hydrodynamics and sedimentation (Allen, 1995; D'Alpaos et al., 2011; French, 1993; Mudd et al., 2009; Rogers et al., 2012; Schile et al., 2014; Stralberg et al., 2011; van Wijnen & Bakker, 2001). Other studies modeled more detailed vegetation-water-land interactions by considering the impact of vegetation density, height, and submergence on water flow and sediment transport (e.g., Da Lio et al., 2013; D'Alpaos et al., 2007; Duvall et al., 2019; Mudd et al., 2004, 2009; Temmerman et al., 2005). *Morris et al.* (2002) first proposed a clear relationship between marsh vegetation biomass and its depth below mean highest tide level based on the field observation on the coastal marsh in South Carolina, USA. Other studies extended this work to explicitly integrate quantitative representations for vegetation dynamics into coastal marsh evolution by assuming 1) a linear relationship between *Spartina*-dominant vegetation and its inundation condition (Belliard et al., 2015; D'Alpaos et al., 2007), 2) a nonlinear relationship between *Spartina*-dominant vegetation and its inundation condition (Kirwan & Murray, 2007; Mariotti & Fagherazzi, 2010), or 3) a linear relationship between multiple vegetation species and their inundation condition (Belliard

This article is protected by copyright. All rights reserved.

et al., 2015; D'Alpaos et al., 2007, 2019; Marani et al., 2004, 2013; Silvestri et al., 2005). The detailed explanations are presented in Subsection 2.

Many of these modeling studies evaluated the vulnerability of coastal marshes under SLR by using a lumped approach, where they treated coastal marshes as a single point or only focused on the marsh near the seaward boundary without an examination of the marsh spatial variation from the ocean to the upland in responding to SLR (D'Alpaos et al., 2011; French, 2006; Kirwan et al., 2010; Kirwan & Temmerman, 2009; Mudd et al., 2009; Temmerman et al., 2003; van Wijnen & Bakker, 2001). Other studies investigated the spatial and temporal variation of coastal marsh evolution under SLR (D'Alpaos et al., 2007; D'Alpaos & Marani, 2016; Kirwan, Walters, et al., 2016; Marani et al., 2013; Ratliff et al., 2015). However, the response of coastal marsh evolution under SLR to varying representations of vegetation dynamic processes is still not well understood, especially the co-evolution of coastal marsh elevation and vegetation. Furthermore, as the complexity and sophistication of these coastal models continues to increase, there is a critical knowledge gap in how sensitive model predictions are to model parameterizations under different SLR conditions. This knowledge is critical for developing effective model parameterizations, and designing field studies to constrain those model parameters under different SLR scenarios. Currently, this knowledge gap limits our confidence in the application of these types of models to inform coastal wetland management and protection.

In this study, we used a coastal eco-geomorphic model with different vegetation dynamic representations to investigate the eco-geomorphologic feedbacks in coastal marshes under future SLR conditions to address the following two questions:

1) How will the selection of vegetation representations result in spatial and temporal differences in eco-geomorphologic outcomes of coastal marshes under SLR?

This article is protected by copyright. All rights reserved.

Accepted Article

2) How will the different vegetation representations and different rates of SLR affect model parametric sensitivity?

To address these questions we simulated the evolution of a one-dimensional coastal marsh transect using a well-established coastal eco-geomorphologic model from *D'Alpaos et al.* (2007). Specifically, under two commonly-used future global mean SLR scenarios (SLR=0.005 m/yr and SLR=0.01 m/yr, corresponding to RCP (Representative Concentration Pathways) 4.5 and RCP 8.5 scenarios in Phase 5 of the Coupled Model Intercomparison Project (CMIP5) (Spencer et al., 2016), we explored three different dependencies of vegetation biomass on elevation above mean sea-level: linear and non-linear formulations for the *Spartina*-dominant vegetation (D'Alpaos et al., 2007; Mariotti & Fagherazzi, 2010; Morris et al., 2002); and the mixed-species linear function (D'Alpaos et al., 2007). After comparing the spatial and temporal variations of coastal marsh evolution under SLR with different vegetation equations, we used a global sensitivity approach to evaluate the sensitivity of eco-geomorphologic processes to model parameterizations spanning a wide range of the parameters.

The paper begins by introducing process representation in Section 2, followed by model introduction, study site, experiment design, and model setting in Section 3. Then we analyze the marsh evolution and model sensitivity under different rates of sea level rise, vegetation schemes, and maximum organic soil production rates in Section 4. Finally, we discuss the implications of this study for understanding the vulnerability of coastal marsh under SLR, guiding data-model integration, representativeness, and uncertainties.

This article is protected by copyright. All rights reserved.

Accepted Article

2. Background: process representation in eco-geomorphologic models

Eco-geomorphologic models represent topographic change of coastal marsh as the net balance of sediment erosion and deposition (Fagherazzi et al., 2012). Based on mass conservation, the spatially-averaged dynamics of topographic elevation in a coastal landscape can be expressed as

$$\frac{dz}{dt} = \frac{1}{1-p}(D - E) - R, \quad (1)$$

where z is the surface elevation relative to the mean sea level with the dimension of [L]; t is time [T]; p is the porosity of bed sediment; D and E represent local sediment deposition and erosion rates with the dimensions of [LT^{-1}], respectively; and R is the rate of sea level rise [LT^{-1}].

However, the way each term in Eq. 1 is modeled may vary. For the erosion term (E) in Eq. 1, it may consist of erosion due to bed shear stress induced by currents and waves and/or due to wave breaking (Carniello et al., 2005; Marani et al., 2010; Mariotti & Fagherazzi, 2010; Van Rijn, 1993), namely,

$$E = E_{shear} + E_{break}, \quad (2)$$

where E_{shear} is the erosion due to bed shear stress [LT^{-1}]. Erosion occurs when the bed shear stress (τ_0) exceeds the critical shear stress for erosion (τ_e), viz

$$E_{shear} = \begin{cases} \alpha\left(\frac{\tau_0}{\tau_e} - 1\right) & if\ \tau_0 > \tau_e \\ 0 & if\ \tau_0 < \tau_e \end{cases}, \quad (3)$$

This article is protected by copyright. All rights reserved.

where α is the erosion coefficient. E_{break} in Eq. 2 is the erosion due to wave breaking [LT^{-1}]. According to *Mariotti and Fagherazzi* (2010), E_{break} is a function of wave power dissipated by breaking:

$$E_{break} = \begin{cases} \beta \left(\frac{P}{P_{cr}} - 1 \right) / d & if\ P > P_{cr} \\ 0 & if\ P < P_{cr} \end{cases}, \quad (4)$$

where β is the wave erosion coefficient; P is the wave power per unit area [$WT^{-1}L^{-2}$]; P_{cr} is the threshold of wave power for wave erosion [$WT^{-1}L^{-2}$]; and d is the spatial interval over which wave breaking occurs [L].

The sedimentation rate, D in Eq. 1, is given by

$$D = D_s + D_t + D_o, \quad (5)$$

where D_s is the inorganic sediment settling rate [LT^{-1}], which is a function of settling velocity (w_s) [LT^{-1}] (Cao et al., 2020), suspended sediment concentration (C), bed shear stress (τ_0) due to water flow [$ML^{-3}T^{-2}$], and critical shear stress for sedimentation (τ_d) [$ML^{-3}T^{-2}$] (Krone, 1962), namely,

$$D_s = \begin{cases} w_s C \left(1 - \frac{\tau_0}{\tau_d} \right) & if\ \tau_0 < \tau_d \\ 0 & if\ \tau_0 > \tau_d \end{cases}. \quad (6)$$

D_t in Eq. 5 is the inorganic sediment trapping rate due to the effect of vegetation canopy [LT^{-1}], which can be represented by an empirical form

$$D_t = CU\epsilon d_s n_s \min[h_s, h_w] \quad (7)$$

where U is the water flow velocity [LT^{-1}]; ϵ is a capture efficiency of vegetation stems, h_w is the water flow depth [L], and several vegetation characteristics, such as plant stem diameter (d_s), stem density (n_s), and vegetation height (h_s) (Mudd et al., 2004; Palmer et al., 2004).

This article is protected by copyright. All rights reserved.

Accepted Article

Additionally, D_o in Eq. 5 is the organic matter production rate [LT^{-1}], which is a function of plant biomass, viz

$$D_o = K_b \frac{B}{B_{max}}, \tag{8}$$

where K_b is the maximum production rate of belowground organic material [LT^{-1}]; B is the aboveground plant dry biomass at the current time [ML^{-2}]; and B_{max} is the maximum vegetation biomass [ML^{-2}]. The growth of coastal marsh vegetation is controlled by several factors related to nutrient inputs (e.g., nitrogen and phosphorous) and soil environmental stress (e.g., oxygen availability, salinity, and sulfide concentration) (Silvestri & Marani, 2004). *Morris et al.* (2002) proposed a relation between vegetation biomass and the depth of the marsh surface below the mean highest tidal level based on observations at a coastal marsh in South Carolina, USA. Based on this relation, several empirical functions were derived to represent equilibrium vegetation biomass under different ponding conditions. The empirical function can be expressed as a linear (D'Alpaos et al., 2007) or a parabolic (Morris et al., 2002) function of salt marsh elevation relative to tide level. For the linear dependency, the lowland area with frequent flooding is more favorable for salt-tolerant and flood-tolerant species, such as *Spartina alterniflora*. The vegetation biomass is proportional to inundation depth. Quantitatively, the biomass equation can be written as (see the blue line in Fig. 2)

$$B_1 = \begin{cases} \left(\frac{MHTL - D_{biomin} - z)}{D_{biomax} - D_{biomin}}\right) B_{max} & if\ MHTL - D_{biomax} \le z \le MHTL - D_{biomin} \\ 0 & if\ MHTL - D_{biomax} > z\ or\ z > MHTL - D_{biomin} \end{cases}, \tag{9}$$

where B_1 is the time-averaged aboveground biomass density [ML^{-2}]; B_{max} is the maximum biomass density [ML^{-2}]; $MHTL$ represents the mean highest tide level [L]; D_{biomax} and D_{biomin} are the highest and lowest depth below *MHTL*, respectively, which bounds the upper and lower

This article is protected by copyright. All rights reserved.

limits of vegetation growth range (D'Alpaos et al., 2007). $MHTL - D_{biomin}$ and $MHTL - D_{biomax}$ represent the elevations of the upper and lower boundaries for vegetation growth (the dashed lines in Fig. 2). Whereas, some mixed species on marshland prefer higher elevation region with less flooding and better aerated soil (see the orange line in Fig. 2), namely

$$B_2 = \begin{cases} 0 & if\ MHTL - D_{biomax} > z \\ \left(\frac{z-(MHTL-D_{biomax})}{D_{biomax}-D_{biomin}}\right) B_{max} & if\ MHTL - D_{biomax} \le z \le MHTL - D_{biomin} \\ B_{max} & if\ z > MHTL - D_{biomin} \end{cases}, \quad (10)$$

where B_2 is the time-averaged aboveground biomass density for mixed species [ML^{-2}] (D'Alpaos et al., 2007). Besides these linear functions, a parabolic formulation describes that the plant biomass goes to zero when the marsh surface elevation reaches the upper ($MHTL - D_{biomin}$) or lower bound ($MHTL - D_{biomax}$), and the biomass reaches its peak at a certain elevation between $MHTL - D_{biomin}$ and $MHTL - D_{biomax}$ (see the yellow line in Fig. 2):

$$B_3 = \begin{cases} 0 & if\ MHTL - D_{biomax} > z\ or\ z > MHTL - D_{biomin} \\ B_{max}(aD + bD^2 + c) & if\ MHTL - D_{biomax} \le z \le MHTL - D_{biomin} \end{cases}, \quad (11)$$

where B_3 is the time-averaged aboveground biomass density [ML^{-2}] (Morris, 2006); D is the ratio between $MHTL - D_{biomin} - z$ and $D_{biomax} - D_{biomin}$; *a*, *b*, and *c* are fitting coefficients.

[Approximated location of Figure 2]

The representation of marsh hydrodynamics driven by tides and waves is also an essential part of eco-geomorphologic modeling because both erosion and sedimentation are fundamentally tied to surface water flow (Scheidegger, 1961). The shallow water equations, derived from the depth-integrated Navier–Stokes equations, have been widely used to compute hydrodynamics in coastal regions where the water horizontal length scale is much greater than the vertical length scale (Vreugdenhil, 2013). Specifically, the shallow water equations consist

This article is protected by copyright. All rights reserved.

Accepted Article

of two conservation equations: 1) conservation of mass and 2) conservation of momentum. Namely, in a one-dimensional (1-D) domain,

$$Conservation\ of\ mass\text{:}\ \frac{\partial \eta}{\partial t} + \frac{\partial (\eta u)}{\partial x} = 0, \tag{12}$$

and

$$Conservation\ of\ momentum\text{:}\ \frac{\partial u}{\partial t} + u\frac{\partial (u)}{\partial x} = -g\frac{\partial (h)}{\partial x} - g\frac{u|u|}{C^2 h} = 0, \tag{13}$$

where h is the water surface elevation = land surface elevation (z) + local water flow depth (η) [L], thus h varies not only depending on the change in water depth, but also the simultaneous morphological change; u is the flow velocity [LT^{-1}]; g is the gravitational acceleration [LT^{-2}]; x is the spatial direction along the 1-D domain [L]; and C is the Chezy's friction coefficient.

3 Methodology

3.1 Numerical model

We used a 1-D version of the coastal eco-geomorphologic model developed by *D'Alpaos et al.* (2007) (hereinafter referred to as D-model) focusing on the interaction between land and ocean without lateral water and sediment fluxes, such as tidal channels. The D-model integrates all the hydro-eco-geomorphologic components introduced in Fig. 1, including sediment settling (Eq. 6), sediment trapping (Eq. 7), vegetation organic matter production (Eq. 8), and sediment erosion due to tidal currents (Eq. 3), except sediment erosion due to waves because the effect of waves in controlling the spatial and temporal variation of coastal marsh evolution was well studied by *Duvall et al.* (2019) and *Mariotti and Fagherazzi* (2010), and vegetation can significantly mitigate waves if the waves are not too strong, thus wave-induced erosion is not a focus in this study. We focused on conditions with regular semi-diurnal tidal

This article is protected by copyright. All rights reserved.

Accepted Article

Accepted Article

cycle and background SLR. For the representation of vegetation biomass, the original D-model included functions (e.g., Eqs. 9 and 10) that assume a linear relationship between annual averaged biomass and the elevation relative to mean sea level and considered different responses of *Spartina* and mixed vegetation species (see details in Section 2). To have a comprehensive understanding of the differences of the eco-geomorphologic feedbacks under different representations of vegetation dynamics, we incorporated the nonlinear function (e.g., Eq. 11) into the D-model as well. For the computation of hydrodynamics, the D-model uses an approach similar to the kinematic-wave form that assumes a balance between water surface slope and friction in the momentum equation (Eq. 13) (D'Alpaos et al., 2007; Rinaldo et al., 1999). The detail of the hydrodynamic component is referred to the supplementary information Text. S1 and *D'Alpaos et al.* (2007), and the detail for the sediment transport component is referred to Section 2 above and *D'Alpaos et al.* (2007).

3.2 Numerical Experiment

We used a 1-D transect based on a marsh platform along the Delaware Bay, USA, as a prototype for our simulations (the black solid line in Fig. 3c). Marsh surface elevation in the 1-D transect is at a level close to the mean highest tide level (MHTL, gray dashed line in Fig. 3c), consistent with observations in Delaware Bay based on the CoNED coastal elevation database (Danielson et al., 2016) and NOAA (National Oceanic and Atmospheric Administration) tide observations (NOAA, 2001), which indicates that the landscape is at or close to an equilibrium state under the current sea level conditions (D'Alpaos et al., 2007).

This study simplifies the 1-D transect topography by using a linear interpolation of the observed topography (red line in Fig. 3c) as the initial land surface elevation for the numerical experiments. The origin of the 1-D model domain is placed at the seaward boundary (x=0),

This article is protected by copyright. All rights reserved.

whereas the upland boundary is located at x=L. Water and sediment can only flow through the seaward boundary with zero flux flowing through the upland boundary. The current mean sea level (MSL) is at -0.13 m above NAVD88 (North American Vertical Datum of 1988), and the averaged tide amplitude is about 0.8 m based on the NOAA tide and current observation at station Cape May, NJ [8536110] (the red star in Fig. 3b). We used a constant suspended sediment concentration (C_0=20 mg/L) at the ocean boundary (x=0). The value of C_0 falls at the lower bound of the range of sediment concentration used in the previous coastal eco-geomorphologic modeling studies (e.g., Kirwan, Walters, et al., 2016). Thus, this study makes a conservative prediction of coastal marsh change under SLR. However, a comparable numerical experiment with the same model settings but with a higher suspended sediment concentration (C_0=100 mg/L) was also conducted, and the results can be found in the supplementary information (see Figs. S2 and S3).

[Approximated location of Figure 3]

In order to speed-up simulations to geomorphologically relevant time scales, the simulations adopted a morphological scaling factor (MSF, e.g., *Lesser et al.* (2004); Roelvink (2006); Zhang et al (2016)), which effectively assumes that changes in the topographic profile over time scales smaller than the scaling factor do not appreciably affect the flow field and the eco-geomorphic dynamics. Hence, elevation change is computed offline by applying sediment fluxes determined in a tidal cycle, assumed to be constant for a period of time equal to the MSF. Thus, in this study, the simulations were run for 500 years (consistent with the simulation time in *D'Alpaos et al.* (2007) to make sure the landscape reaches an equilibrium state) with a spatial interval of 1 m and a time interval of 10 minutes for hydrodynamics in a single tidal cycle and

This article is protected by copyright. All rights reserved.

MSF=50 for the eco-geomorphologic change of 50 tidal cycles. The same numerical settings were applied to the M-model simulations in the supplementary information.

We designed several focused numerical experiments to characterize eco-geomorphologic feedbacks under different representations of vegetation dynamics and SLR scenarios for the future 500 years. We adopted two commonly used future global mean SLR scenarios from global climate model predictions, including (1) the relatively low SLR rate (0.005 m/yr) (Da Lio et al., 2013; Ganju et al., 2020; Kirwan & Temmerman, 2009; Spencer et al., 2016) and (2) the relatively high rate of SLR (0.01 m/yr) (Ganju et al., 2020; Kirwan, Walters, et al., 2016; Orson et al., 1985; Spencer et al., 2016). In addition, we considered three different representations of vegetation dynamic processes, such as the *Spartina*-dominant linear function, *Spartina*-dominant nonlinear function, and mixed species linear function. Also, in simulating vegetation organic soil production, we incorporated two different rates of maximum organic production rates: 1) $K_b = 0.003\ m/yr$, a commonly used maximum organic production rate under current climate (Langley et al., 2009; Morris et al., 2016) and 2) $K_b = 0.005\ m/yr$, a larger maximum organic production rate, reflects the increase of belowground biomass productivity under elevated atmospheric CO_2 in the future (Ratliff et al., 2015). Specifically, based on a comprehensive literature review, *Ratliff et al. (2015)* found that biomass productivity increased about 33% for a 400 ppm increase in atmospheric CO_2. Here, we assumed a present-day maximum organic production rate of 3 mm/yr. Under the RCP 8.0 climate scenario (the most ambicis future CO_2 emission scenario), the CO_2-equivalent levels was projected to exceed 1200 ppm, which means an additional 800 ppm with respect to present (Hayhoe et al., 2017). This leads to a future maximum organic production rate equal to 0.00498 m/yr $\approx$ 0.005 m/yr.

This article is protected by copyright. All rights reserved.

Accepted Article

Scenario details are listed in Table 1. The parameters for these individual simulations are listed in the fourth column in Table 2.

[Approximated location of Table 1]

3.3 Sensitivity analysis

There are many sensitivity analysis approaches available to understand parametric sensitivity of model behavior (see *Song et al*. (2015) for a detailed review). In this study, we used a widely applied sensitivity analysis approach, the Fourier Amplitude Sensitivity Test (FAST) technique (Cukier et al., 1973; Xu & Gertner, 2011, 2008a). FAST is computationally efficient and can be used for both nonlinear and non-monotonic relationships between parameters and model outputs (Xu & Gertner, 2011). FAST uses a periodic sampling strategy to assign a characteristic periodic signal for each parameter. Within FAST, a Fourier transformation is used to decompose the variance in model outputs into partial variance contributions by individual model parameters based on the assigned signals. The ratio of partial variance contributed by a specific parameter to the total variance of a model output is defined as the first-order sensitivity index to measure the importance of each model parameter. The FAST analysis has been incorporated into a software tool, the UASA ToolBox (https://sites.google.com/site/xuchongang/uasatoolbox) by *Xu and Gertner (2008b)* and provides a rigorous way of defining, executing, and analyzing experiments for model parametric sensitivity.

This study selected 11 common parameters that have been used in many coastal eco-geomorphologic models (see the list of the parameters in Table. 2). Based on this selection, the UASA ToolBox was used to generate 1,100 groups of parameters for the model ensemble

This article is protected by copyright. All rights reserved.

Accepted Article

simulations to quantify the models' individual parametric sensitivities. The range of each parameter is estimated based on our literature survey and empirical knowledge. However, because there is not enough data to derive informative probability density distributions, we used a uniform distribution for our sensitivity analysis.

Model sensitivity is defined in terms of relevant quantitative metrics describing the final state of the system: 1) the difference between the MHTL and the elevation at the seaward boundary (MHTL minus elevation, hereinafter referred to as *Depth_m*), 2) the difference between minimum and maximum elevations (hereinafter referred to as elevation relief) from each ensemble simulation under different scenarios, 3) domain averaged sediment fluxes, 4) the vegetation biomass at the seaward boundary, and 5) the vegetation biomass at the upland boundary. Notably, the first metric, *Depth_m*, measures how the landscape elevation (at least the seaward boundary) responds to SLR. While the second metric (elevation relief) measures the difference of elevation at the seaward boundary and inland and possible inland depression on the 1-D marshland.

[Approximated location of Table 2]

4. Results

4.1 Topographic evolution and sediment fluxes under different SLR rates

4.1.1 Topographic change across individual simulations

We first used the twelve individual simulations (cases 1 to 12 in Table. 1) as examples to compare the elevation change under different vegetation equations for biomass estimation and SLR scenarios simulated by the D-model over 500 years (see Fig. 4). The corresponding sediment fluxes at the end of the 500 years are illustrated in Fig. 5. Domain-wide, the elevations

This article is protected by copyright. All rights reserved.

Accepted Article

in the cases with a higher maximum organic production rate (K_b) (the first column in Fig. 4) were higher than the elevation in the lower K_b cases (the second column in Fig. 4). At the seaward boundary, the relative locations between elevation and MHTL near the seaward boundary in all vegetation-covered scenarios remained constant after 400 years' simulation (not shown at here) due to a balance between sediment fluxes (Fig. 5), which indicate that 1) the elevations near the seaward boundary reached a new equilibrium state under future SLR and 2) the marshland near the seaward boundary kept pace with the rates of SLR. In contrast, the cases without vegetation showed clear declines of elevation near the ocean boundary (gray dashed lines in Fig. 4) due to erosion (the black lines in Fig. 5d and k) and lack of organic accretion and inorganic trapping. The final elevations with vegetation coverage reached the level of MHTL (solid lines in Fig. 4), except in the high SLR and low K_b scenario (Fig. 4c), where the elevation was 0.2-0.3 m below the MHTL, and in the low SLR and high K_b scenario (Fig. 4b), where the simulated marsh surface elevation with the mixed-vegetation equation (hereinafter referred to as mixed-veg case) was equal to the MHTL because the organic production rate is equal to the SLR (see the sediment flux in Fig. 5j).

Moving landward, the marsh elevations declined due to a decrease in sedimentation rate landward. Some of the marshland became totally submerged in water as the elevation was below the final mean sea level (final MSL indicated by the blue dashed lines in Fig. 4). With a higher K_b, a shorter portion of the marshland was below the final MSL because a higher K_b resulted in a higher organic sedimentation rate, which dominantly contributed to the accretion rate at the upland area where inorganic sediment from the ocean was restricted to this region.

High SLR caused a larger elevation relief up to 5m (Figs. 4a and c), compared to the low SLR scenarios that only had a maximum elevation relief of 0.48 m in the higher K_b case

This article is protected by copyright. All rights reserved.

(Fig. 4b) and 2.85m in the lower K_b case (Fig. 4d), respectively. Notably, in the lower SLR scenario with a higher K_b, the elevation only slightly declined landward (Solid lines in Fig. 4b), which means that the accretion rate domain-wide can always keep pace with the rate of SLR as illustrated in Fig. 5h, i, and j.

[Approximated location of Figure 4]

Different vegetation schemes also highlight different influences on the topographic outcomes. Among all the vegetation cases, the *Spartina*-nonlinear case showed the highest final elevation and the least elevation relief due to the highest sedimentation rate throughout the domain, particularly due to organic soil production in the middle and upper portions of the transect. Elevation declined closer to the ocean boundary in the mixed-veg cases than the elevations with *Spartina*-dominant linear and nonlinear functions (hereinafter referred to as *Spartina*-linear case and *Spartina*-nonlinear case, respectively) (thick and thin black solid lines in Fig. 4). Notably, in the mixed-veg case under low SLR and high K_b (gray solid line in Fig. 4b), the elevation reached a level similar to the MHTL. This was because the vegetation growth in the mixed-veg case is greater at lower inundation levels. Thus, vegetation continued growing even when the elevation was at the same level of the MHTL. In the *Spartina*-dominant cases, the *Spartina*-nonlinear cases showed the declines of elevation started closer to the seaward boundary than the elevation decline in the *Spartina*-linear cases (black solid lines in Fig 4a, c, and d).

The simulations with a higher suspended sediment concentration in the ocean (Co=100mg/L), a higher SLR rate (0.01 m/yr), and a higher K_b (0.005 m/yr) showed similar profiles with the simulations under a lower suspended sediment concentration from the ocean: the marsh elevation near the ocean boundary was at the similar level with the future MHTL, and

This article is protected by copyright. All rights reserved.

Accepted Article

the marshland at the upland was drowning (see Fig. S2 in the supplementary information) at the end of the 500 years' simulation. However, with a higher sediment supply from the ocean, we observed a longer portion of the marsh elevation (~300 m from the ocean boundary) can keep pace with the increase of sea level, compared with the elevation profile in the lower sediment concentration cases. The high sediment concentration case also predicted less elevation relief than that in the low sediment concentration case due to a higher sediment supply from the ocean.

For the contributions of sediment fluxes to marshland accretion, in general, sediment settling rate contributed more than sediment trapping rate and organic production rate near the seaward boundary (light blue lines in Fig. 5) in all vegetation-covered cases, except the mixed-veg cases (Figs. 5j and n) where the organic production rate was higher than the other fluxes. This is because the mixed-veg case assumes that vegetation can grow better under lower inundation or no inundation conditions where vegetation organic production always plays a role in contributing to marsh accretion, but inorganic sediment settling contributes less due to limited delivery of sediment landward. Given that the elevation near the seaward boundary accreted faster than the inland area, the inundation depth near the seaward boundary was shallower than the inland, which provided a more favorable condition for mixed vegetation species to grow near the seaward boundary, resulting in a higher organic production rate there.

Moving landward, the inorganic sediment settling rate was still a dominant sediment flux contributing to the accretion rate, except the cases with a lower SLR rate and higher K_b, where the organic production rate was dominant (purple lines in Figs. 5h, i, and j). The spatial patterns of the sediment fluxes reflected the different assumptions of the vegetation schemes. For example, the patterns of fluxes were very different between the mixed-veg cases (the third

This article is protected by copyright. All rights reserved.

row) and *Spartina*-dominant case (the first and second row) due to the different assumptions of the favorable growth condition for vegetation. We did not observe erosion under this regular tidal cycle and sea level rise condition in the vegetation-covered cases because vegetation reduced water flow velocity and prevented erosion in these experiments.

[Approximated location of Figure 5]

4.1.2 Model parametric sensitivity from ensemble simulations

We explored the model parametric sensitivity represented by the ratio of individual parametric variance to the total variance from the ensemble simulations across different combination of parameters spanning wide ranges of their values (see Table. 2).

4.1.2.1 Parametric sensitivity for topographic change

For the sensitivity of modeled *Depth_m* (defined as MHTL minus elevation in Subsection 3.3) to parameterization (Fig. 6a), vegetation-related parameters showed a larger influence on *Depth_m* under the higher SLR rate scenarios (e.g., the first three columns in Fig.6a). While, under the lower SLR rate scenarios, the sediment-related parameters, especially the “sediment concentration”, were the dominant parameters (the last three columns in Fig. 6a). For the different vegetation dynamic schemes, the mixed-veg cases were highly sensitive to the “maximum organic production rate” indicating that the *Depth_m* was highly dependent on the organic matter production rate regardless of the rates of SLR because some species in the mixed-veg cases can grow under more prolonged flooding condition, and the other species are adapted to less frequent and prolonged flooding condition, such that the vegetation processes can contribute to sedimentation in all conditions. While, in the *Spartina*-dominant cases, the vegetation can only grow under more prolonged flooding condition driven by SLR and tide.

This article is protected by copyright. All rights reserved.

Accepted Article

Thus, the parametric sensitivities in the *Spartina*-linear and -nonlinear cases (the first, second, fourth, and fifth columns in Fig. 6a) were controlled by the inundation condition, the sediment settling, and vegetation processes and did not present a huge difference among parameters, compared to the mixed-veg cases. The relatively more sensitive parameters are “maximum organic production rate”, “maximum biomass”, “water depth for plant growth”, “sed concentration”, and “critical shear stress for deposition”. Among these parameters, the “maximum organic production rate” was the most sensitive parameter in the high SLR scenario (the first and second columns inf Fig. 6a). In contrast, “sediment concentration” was the most sensitive parameter in the low SLR scenarios (the fourth and fifth columns in Fig. 6a). This is because the high rate of SLR has a larger potential to cause a higher inundation condition by high tides, a favorable condition for *Spartina* to grow. Therefore, the vegetation effect had a larger contribution to sedimentation than the contribution from vegetation in the low SLR cases.

For the sensitivity of elevation relief, in the high SLR scenario (the first, second, and third columns in Fig. 6b), the model simulations were more sensitive to “sediment diffusivity”, an important parameter in the sediment diffusion equation that controls how much sediment could diffuse landward. “Tide amplitude” was also one of the most sensitive parameters in the *Spartina*-linear and -nonlinear cases. The vegetation-related parameters showed relatively low sensitivity under the higher SLR rate (the first and second columns in Fig. 6b), which means that the elevation relief was more dependent on how much sediment can transport landward and deposit under a high SLR rate. However, in the mixed-veg case, the “maximum organic production rate” along with “sediment diffusivity” were the most sensitive parameters, which reflects the tolerance of the growth of mixed vegetation species in different conditions. For the lower SLR scenario (the fourth to sixth columns), the vegetation-related parameters showed

This article is protected by copyright. All rights reserved.

higher sensitivity, which means that the vegetation processes were more dominant to the change of elevation relief, especially for the *Spartina*-linear and nonlinear cases under a low rate of SLR. The values of sensitivity for each parameter in each scenario can be found in Tables S1 and S2.

[Approximated location of Figure 6]

4.1.2.2 Parametric sensitivity for sediment fluxes

The parametric sensitivities of sediment fluxes to model parameterization are similar to corresponding vegetation cases under both SLR scenarios. For example, the *Spartina*-linear cases (the first to third columns in Fig. 7a and first to third columns in Fig. 7b) under both the high and low SLR scenarios show a similar parametric sensitivity for each corresponding sedimentation processes.

Specifically, for the sediment settling process, all the cases (the first, fourth, and seventh columns in Fig. 7a and the first, fourth, and seventh columns in Fig. 7b) were most sensitive to the "maximum organic production rate", which may be because the organic production influences elevation changes that indirectly control sediment settling process. Besides the "maximum organic production rate", the model simulations were also sensitive to some sediment settling-related parameters, such as "sediment concentration", "settling velocity", and "critical shear stress for deposition", which are the key parameters directly control sediment settling process. For the organic soil production by vegetation, all the cases (the second, fifth, and eighth columns in Fig. 7a and the second, fifth, and eighth columns in Fig. 7b) were most sensitive to the "maximum organic production rate", the key parameter in organic soil production process. For the sediment trapping process, the sensitivity was almost evenly

This article is protected by copyright. All rights reserved.

Accepted Article

Accepted Article

distributed for each parameter because sediment settling, sediment diffusion and advection, and vegetation all influence sediment trapping, however, the parameters of "sediment diffusivity" and "sediment concentration" that control the distribution of sediment concentration showed slightly higher sensitivity. The values of sensitivity for each parameter in each scenario can be found in Tables S3 and S4.

[Approximated location of Figure 7]

4.2 Vegetation dynamics with the change in surface topography

4.2.1 The spatial and temporal variation of vegetation biomass from individual simulations

The different formulations for vegetation growth in response to inundation conditions (illustrated in Fig. 2) lead to distinct patterns in biomass distributions and marsh response to tidal and SLR induced flooding. Figure 8 showed the spatial variation of vegetation biomass at the end of 500 years in the simulations under the different vegetation dynamic schemes, rates of SLR, and K_bs. In general, the spatial patterns of vegetation biomass corresponded to the marsh elevation profiles in Fig. 4. For example, the locations of dramatic declines of vegetation biomass in the high SLR scenarios are well-aligned with the topographical depression area in Fig. 4a and c. In this low-lying region, the marsh elevations approach an unfavorable inundation condition for vegetation growth with high ponding water detrimental to vegetation growth. In contrast, the vegetation biomass even increased landward in the lower SLR and higher K_b scenario because the entire domain kept pace with the SLR rate, and the inundation condition was still within the vegetation's growth range (see the elevation profiles in Fig. 4b). Notably, the vegetation biomass of the mix-veg case reached its maximum biomass across the entire model domain (the gray dashed line in Fig. 8). However, with the lower K_b, the simulation

This article is protected by copyright. All rights reserved.

shows an abrupt decrease when the marshland was submerged in water (Fig. 8d), similar to the final biomass profile in the high SLR scenarios.

For the mixed-veg cases, despite the different locations of the abrupt decreases, they showed similar patterns under the lower K_b (Fig. 8c and d), but different responses under the higher K_b (Fig. 8a and b). In the low SLR condition with the higher K_b (Fig. 8b), the mixed vegetation biomass was relatively uniform and greatly exceeded the linear and non-linear single species simulations across the entire model domain (the gray dashed line). In contrast, under the high SLR and higher K_b scenario (Fig. 8a), the mixed vegetation biomass outpaced the single species within ~100 m from the seaward boundary, but then rapidly decreased landward of this location to zero. The *Spartina*-linear and -nonlinear formulations increased approximately linearly and then decreased to zero at further locations landward, compared with the mixed-veg cases. The *Spartina*-nonlinear cases showed a higher estimated vegetation biomass than the biomass in the *Spartina*-linear cases, but the biomass started to decrease to zero closer to the seaward boundary in the *Spartina*-nonlinear cases, which reflected the nature of the differences in the assumptions in the vegetation equations.

[Approximated location of Figure 8]

In order to examine the temporal evolution of biomass across the marsh, we plotted the time series at three locations: the seaward boundary, and 100 m and 400 m landward of the boundary (Figure 9). Across the 12 simulation cases, the temporal evolution of biomass may be divided into three stages, though not all stages are presented at all locations or every scenario.

Rapid change characterizes the first stage. With the exception of mixed vegetation (Figure 9 c, f, i, and l), all locations exhibited rapid increases in biomass for the first 100 to 200 years of the simulation. During the second stage, biomass continued to adjust but at

This article is protected by copyright. All rights reserved.

Accepted Article

Accepted Article

significantly slower rates than the first stage. These adjustments are seen at the seaward boundary and 100 m locations in the *Spartina*-linear simulations under both SLR forcings and K_b values (orange and cyan circles in Figure a, d, g, and j) and *Spartina*-nonlinear simulations (orange and cyan circles in Figure 9b, e, h, and k). A dramatic exception to the gradual adjustments in Stage 2 is the 400 m location in the *Spartina*-linear and -nonlinear rapid SLR scenarios (green circles in Figs 9a, b, d, and e) and the low K_b scenarios (green circles in Figs. 9d, e, j, and k) in which biomass rapidly drops back to a value of zero between 100 and 300 years.

The third stage is the period when a system enters a stable state or equilibrium state, which indicated that a new equilibrium or quasi-equilibrium state was reached under the new rate of SLR. Examples of this stability include the limited changes in vegetation biomass near the seaward boundary and at the 100 m locations in all the cases. This is because the vertical accretion rate at these locations in all the cases always kept pace with the rates of SLR.

Throughout the entire vegetation evolution process, the *Spartina*-linear and -nonlinear cases predicted higher vegetation biomass at the location 100 m from the seaward boundary and lower vegetation biomass near the seaward boundary. Conversely, the mixed-veg cases predicted a higher vegetation biomass near the seaward boundary and lower vegetation biomass at the location 100 m from the seaward boundary. This difference demonstrated the difference in the assumption of favorable inundation conditions in the single-species and mixed-species vegetation equations.

[Approximated location of Figure 9]

This article is protected by copyright. All rights reserved.

Accepted Article

4.2.2 Parametric sensitivity for vegetation dynamics

After analyzing the spatial and temporal variation of vegetation biomass change, we computed the sensitivity of biomass estimation at the seaward boundary and upland boundary to model parameterization based on the ensemble simulations. The biomass estimations were more sensitive to the vegetation-related parameters, especially the parameters of "maximum organic production rate" and "maximum biomass" (Fig. 10). For the vegetation biomass at the upland (the second, fourth, and sixth columns in Fig. 10a and b), "maximum organic production rate" and "maximum biomass" were the two most dominant parameters that control the estimation of biomass. However, the vegetation biomass near the seaward boundary was also sensitive to sediment settling-related parameters. Specifically, in the higher SLR scenario, the biomass estimations near the seaward boundary (the first, third, and fifth columns in Fig. 10a) were also sensitive to all the other parameters, except the parameters for erosion (e.g., "erosion coefficient"). In contrast, in the low SLR scenario, the most sensitive sediment settling-related parameters were only "sediment concentration" and "settling velocity" in the *Spartina*-dominant cases (the first and third columns in Fig. 10b). The vegetation biomass estimation near the seaward boundary in the mixed-veg case was more sensitive to "maximum biomass" and "maximum organic production rate" than the rest parameters. The values of sensitivity for each parameter in each scenario can be found in Tables S5 and S6.

[Approximated location of Figure 10]

This article is protected by copyright. All rights reserved.

Accepted Article

5 Discussion

5.1 Coastal marsh vulnerability under accelerating SLR

5.1.1 Will coastal marsh survive under future SLR?

Our numerical experiments examined the spatial and temporal variation of coastal marsh evolution under three different representations of vegetation dynamic processes. The results presented similar features of final elevation profiles under the three vegetation schemes: 1) the elevation near the seaward boundary kept pace with both the high and low SLR rates (e.g., 0.01 m/yr and 0.005 m/yr) and the high and low K_b (0.005 m/yr and 0.003 m/yr), even with a conservative sediment concentration (e.g., C_0=20 mg/L) at the seaward boundary (Fig. 4) and 2) the elevation landward declined and part of it drowned in water for the high SLR scenarios and low SLR with low K_b. The elevation near the seaward boundary started to approach a new equilibrium state under the rising SL conditions around 100 years (e.g., the cyan circles in Fig. 9a, b, d, e, g, h, j, and k), which was consistent with the findings in previous studies (D'Alpaos et al., 2011; Kirwan et al., 2008; Kirwan, Temmerman, et al., 2016; Kirwan & Temmerman, 2009; Temmerman et al., 2003; van Wijnen & Bakker, 2001). This pattern of lower accretion rates in the interior of marshes has been previously documented in both modeling (D'Alpaos et al., 2007, 2019; Kirwan, Walters, et al., 2016; Langston et al., 2020; Marani et al., 2013; Mariotti, 2016; Ratliff et al., 2015; Thorne et al., 2018) and field studies (Friedrichs & Perry, 2001; Palinkas & Engelhardt, 2019; Schepers et al., 2017; Temmerman et al., 2003). Eventually, the interior marshland died-off and turned into water pools as shown in Fig. 9 (especially the temporal change of biomass at the 400 m location). *Schepers et al.* (2017) also

This article is protected by copyright. All rights reserved.

reported that the size of water pools would expand through time, influencing the connectivity between marshland and channels.

Under climate change, if the maximum organic soil production rate (K_b) increases to a similar level as the rate (0.005 m/yr) used in this study due to the increase of temperature and CO_2 in the future , the spatial and temporal variations of vegetation biomass are relatively small and vary within the vegetation growth range (Figs. 8b and 9g, h, and i) under the lower SLR rate (0.005 m/yr). Based on these results, a SLR of 0.005m/yr does not appear to threaten the survival of coastal marsh systems characterized by these types of vegetation on a 500-year scale. However, for a K_b rate commonly observed today (0.003m/yr), all the SLR scenarios showed clear declines of surface elevation starting near the middle or upper of the domain (solid lines in Fig. 4a) and continuing to the upland boundary illustrating that the accretion rate at the inland portion of the coastal marsh cannot keep pace with the future SLR rates. These inland areas turned into open water habitats with degradation and marsh vegetation mortality occurring after 200-300 years in these locations (Figs. 8a and 9a and b), which may lead to the change of coastal marsh ecosystem functions and hydrological regime shift (Ganju et al., 2020).

The simulations above used a conservative sediment concentration rate from the ocean boundary (C_0=20 mg/L), which limited the delivery of sediment landward under the high SLR rate, resulting the drowning of upland marsh. However, in our simulations with a higher sediment concentration from the ocean (C_0=100 mg/L), more sediment entered the domain and improved the potential for survival of coastal marshland under a high rate of SLR. However, simulations with the higher sediment concentration delayed, but didn't prevent upland submergence, which further demonstrated that coastal marsh is largely vulnerable under the high rate of SLR (0.01 m/yr) (see Figs. S2 and S3 in the supplementary information). A

This article is protected by copyright. All rights reserved.

Accepted Article

microtidal regime (tidal range =1.6 m) was used in the individual simulations. However, the elevation profile would be subject to change under various tidal conditions because different tidal conditions would cause different inundation conditions that would results in distinct marsh vertical accretion. The role of different tidal regime in controlling marsh evolution was also demonstrated by our ensemble sensitivity analysis, where we identified the "Highest tide amplitude" as one of the most sensitive parameters for elevation relief (e.g., Fig. 6b).

5.1.2 Marsh vulnerability due to vegetation representation

The experimental cases with different vegetation schemes consistently predicted coastal marsh vulnerability under future SLR. Under a conservative sediment concentration from the ocean (C_0=20 mg/L), at the seaward boundary, marsh elevation accretion should keep pace with future SLR, regardless the rate of SLR and K_b values. Landward, the inland part of the coastal marsh was resilient under the lower rate of SLR (0.005m/yr) and simultaneously with the higher K_b, but potentially vulnerable to collapse under high rate of SLR or with the lower K_b.

Our simulations also highlighted marsh response to increased ponded water depth under future SLR. The mixed-veg scheme was the most resilient scenario under the lower SLR and with the higher K_b (gray solid line in Fig. 4b): the marsh accretion rate was equal to the SLR rate throughout the entire domain due to less inundation condition and high organic soil production rate. However, the mixed-veg scheme was the most vulnerable scenario under the higher SLR or with the lower K_b (see the mixed-veg cases in Figs. 4 and 8): the decline of marsh elevation started closer to the seaward boundary due to unfavorable high inundation conditions for vegetation growth. Except for the mixed-veg case under the lower SLR and higher K_b, the *Spartina*-nonlinear scheme was the most resilient scheme in all cases—it predicted the largest elevation increases throughout the domain, the least elevation depression

This article is protected by copyright. All rights reserved.

(Fig. 4), and the highest vegetation biomass (Fig.8). These most resilient predictions from the *Spartina*-nonlinear treatment were attributed to the assumption of the nonlinear relationship between vegetation biomass and inundation condition. Vegetation biomass reaches its peak when the inundation depth is at the middle level or near the middle level of the vegetation growth range (defined by the D_{biomax} and D_{biomin}) and does not have to be at the highest inundation level, compared with the *Spartina*-linear scheme. However, we also found that the elevation and vegetation biomass started to decrease closer to the seaward boundary in the *Spartina*-nonlinear case, compared with the *Spartina*-linear case, which implies that the *Spartina*-nonlinear case predicted a bit higher unvegetated□vegetated marsh ratio (UVVR) as defined in *Ganju et al. (2017)*.

In addition, our simulation depicted the evolution of vegetation biomass with the evolution of marsh landscape (Fig. 9), reflecting some of the plant life-history traits (Schwarz et al., 2018). The vegetation biomass of our studied marshland varied through different trajectories at the seaward boundary, mid-marshland, and the upland (Fig. 9). In general, vegetation biomass at the seaward boundary and mid-land reached an equilibrium state at around 100-200 years and dropped dramatically at the upland with the drowning of marshland, revealing the different vegetation responses at different location to boundary drivers and geomorphological change. Notably, the mixed-vegetation scheme predicted that vegetation landward would die out quicker under the high SLR rate (Fig. 9c) than the vegetation in the other vegetation cases. The similarity and distinction of vegetation evolution represented by the different vegetation schemes can potentially describe different vegetation colonization behaviors and cross-species competition during the evolution of coastal marsh (D'Alpaos et al., 2019; Schwarz et al., 2018).

This article is protected by copyright. All rights reserved.

Accepted Article

5.2 Implication to data-model integration and future coastal eco-geomorphologic modeling

Our sensitivity analysis captured the overall parametric sensitivity of the eco-geomorphologic processes in the model and highlighted how different representations of vegetation dynamics and SLR conditions affect the parametric sensitivity. We found that the "sediment concentration" and "tidal amplitude" are the most sensitive parameters for coastal marsh evolution, which are in agreement with the findings in prior studies (D'Alpaos et al., 2007; Kirwan et al., 2010; Kirwan, Walters, et al., 2016; Temmerman et al., 2003). More importantly, this study also identified additional parameters that are highly sensitive for the spatial and temporal variations of key landscape characteristics, such as 1) the *Depth_m* (depth between MHTL and marsh elevation at the seaward boundary), 2) elevation relief, 3) averaged sediment fluxes, and 4) vegetation biomass near the seaward boundary and at the upland. These parameters include "sediment diffusivity", "maximum organic production rate", and "maximum biomass". Thus, this sensitivity analysis highlights the need for future modeling and field observations to better measure and parameterize these controls on marsh evolution.

In particular, our sensitivity analysis identified the parameter of "sediment diffusivity" as one of the most sensitive parameters for predicting marshland evolution, especially controlling elevation relief, which implies the importance of hydrodynamic process that brings water and sediment landward and back to ocean. Although the evaluation of coastal hydrodynamics is outside the scope of this study, a good representation of coastal hydrodynamics as a function of coastal boundary condition (e.g., tide and wave), topographic gradient, and vegetation effect (e.g., influencing surface roughness) is critical for predicting sediment budget accurately and is worth deeper investigation in future modeling studies (Best et al., 2018; Duvall et al., 2019).

This article is protected by copyright. All rights reserved.

Accepted Article

5.3 Representativeness of the model simulations

In this study, we selected the parameter values and the rates of SLR that were widely used in previous modeling studies or were established in the literature from field measurements to ensure that the simulations were realistic and representative. Additionally, the formulations used to represent the dominant processes were selected from broadly used sedimentation, erosion, and vegetation dynamic equations. Thus, the individual simulations should reflect current model capabilities and formulations used to understand process interactions and marsh response to SLR. Based on the ensemble simulations, we generated a large number of parameter samples for the sensitivity analysis. Thus, the results of the sensitivity analyses reasonably reflected the overall sensitivity of the model processes over their physical parameter ranges.

To further demonstrate that the D-model appropriately captures the behavior of coastal evolution under SLR, we conducted some of the same simulations by using another well-established coastal eco-geomorphologic model developed by *Mariotti and Fagherrazi* (2010) (hereinafter referred to as M-model). Similar to the D-model, the M-model integrates all the hydro-eco-geomorphological components introduced in Fig. 1, including sediment settling (Eq. 6), sediment trapping (Eq. 7), vegetation organic matter production (Eq. 8), and sediment erosion due to tidal currents (Eq. 3), as well as sediment erosion due to waves (Eq. 4). To make the simulations by the D- and M-model comparable, we turned off the process of erosion due to waves in the M-model, but kept the process of erosion due to tidal currents. For the representation of vegetation biomass, the M-model only integrated the *Spartina*-dominant nonlinear function as the original model was developed. An introduction to the M-model may be referred to the Text. S2 in the supplementary information and *Mariotti and Fagherazzi*

This article is protected by copyright. All rights reserved.

Accepted Article

(2010), and its simulation results can be found in Figs S4 to S8. The simulations from the M-model showed consistent topographic outcomes and vegetation biomass distribution with the D-model simulations under different rates of SLR and Spartina-nonlinear scheme (M-model only uses the Spartina-nonlinear scheme) (see Figs. S4 to S7). The simulations from the M-model also identified similar most sensitive parameters for different scenarios. For example, the sensitivity of *Depth_m* in the M-model to vegetation-related parameters also increased with the SLR rates. The most sensitive parameters for elevation relief under the higher SLR were also "sediment diffusivity", "sed concentration", and "Highest tide amplitude". The "maximum organic production rate" was a more dominant parameter for elevation relief under the lower SLR. Meanwhile, the most sensitive parameters for sediment fluxes and vegetation biomass were also the "maximum organic production rate" and "maximum biomass".

Both the D- and M-models predicted the elevation relief of marshland under the higher SLR (0.01 m/yr) was up to 2.5 to 5 meters (Figs. 4a and 4c and Fig. S4). This is an accumulative effect of the different accretion rate between the marsh near the ocean boundary and the interior marsh over the 500-year scale, which reflected the model behaviors under different process representations, parameters, and external drivers. It also highlighted the transition zone between more resilient marshland near the river/ocean boundary and more vulnerable interior marsh. Future work is needed to validate the reality of this transition zone with a better field measurement of sedimentation, vegetation biomass, and other marsh accretion-related parameters in these areas.

5.4 Uncertainties and future work

We used two maximum organic production rates (0.003 m/yr and 0.005 m/yr) in the individual simulations in this study. The former one was adopted from the previous studies by

This article is protected by copyright. All rights reserved.

Langley et al. (2009) and Morris et al. (2016), representing an averaged value of the maximum production rate under the present climate condition. The latter one was calculated based on *Ratliff et al*. (2015) and the adoption of the IPCC highest CO_2 emission scenario (Hayhoe et al., 2017), reflecting an increase of vegetation belowground organic production rate under a warming climate. The use of both rates illustrated model parametric sensitivity and the role of organic sedimentation in controlling future marsh elevation change. However, there are still some uncertainties that may affect the organic production rate under a warming climate. On the one hand, the models did not consider the increase of organic soil decomposition rate under the warming climate, which could be comparable or even higher than the organic production rate (Kirwan & Blum, 2011; Langley et al., 2009). On the other hand, it is possible that the soil organic decomposition rate won't increase much due to the constraint from soil aeration level, a factor controlling soil organic decomposition (Roner et al., 2016; Silvestri & Marani, 2004). Therefore, the balance/imbalance between organic soil production and decomposition will be the key to a better understanding of organic accretion in coastal marsh evolution. Thus, future work should focus on better quantifying the organic accretion components (organic soil production and decomposition), as well as the drivers and limits that control these components.

Our sensitivity analysis showed the importance of "maximum biomass" and "organic production rate" for the prediction of marshland elevation changes. Within most of the current eco-geomorphologic models, they are fixed through time. However, future climate changes, higher temperature and CO_2 conditions might change the value of these parameters gradually in the evolution process. Therefore, to improve the prediction accuracy, it is critical to have process-based models that can incorporate the impact of a dynamic future climate on vegetation production and litter decomposition through time.

This article is protected by copyright. All rights reserved.

Accepted Article

Accepted Article

The simulations used a no-flow boundary condition at the upland boundary, which limits the water and sediment supply from uplands through upland surface and subsurface environments. An appropriate consideration of the hydrologic and geomorphologic connectivity with the upland region may improve the flexibility of our test model in realistically representing a wider variety of settings, in terms of the relevant hydrodynamic and sediment transport processes (Wohl et al., 2019; Zhang et al., 2018), especially for intertidal areas receiving water and sediment from both riverine and ocean sources (Gleichauf et al., 2014; Kirwan, Walters, et al., 2016; Wolfram et al., 2016; Yousefi Lalimi et al., 2020). Also, water and sediment fluxes from tidal channel to marshland were not considered in these 1-D simulations. Tidal channel can compensate for the spatial discrepancy in sediment accretion by routing water and sediment from upstream to the coastal area or from the ocean boundary to the upland (Belliard et al., 2016). At the seaward boundary, the models used constant sediment concentration in rivers/ocean, while variability in this concentration could contribute to the uncertainty in predictions of the accretion rate on coastal marshes. In addition, a more precise estimation of sediment concentration in the aquatic systems by using high resolution field measurements or a high-resolution, process-based coastal ocean model would improve the predictive capability of coastal marsh eco-geomorphologic models (Stumpf, 1983; Temmerman et al., 2003).

6 Conclusion

We used a coastal eco-geomorphologic model with different vegetation dynamic representations to investigate eco-geomorphologic feedbacks on the coastal marsh and changes in model parametric sensitivity under various future SLR conditions. We conducted model simulations by using a standard set of test cases with consistent model settings and parameters. This study explored coastal marsh evolution under SLR not only from the domain averaged

This article is protected by copyright. All rights reserved.

Accepted Article

features, but also from the spatial and temporal variations of key landscape characteristics, such as the elevation relief and biomass at the seaward boundary and upland. We found that evaluating the spatial and temporal coastal marsh evolution under different representations of vegetation dynamic process provides new insights to better understanding the uncertainty of predicting coastal marshes vulnerability facing future accelerating SLR from different process representations.

Qualitatively, the three vegetation dynamic schemes (*Spartina*-linear, *Spartina*-nonlinear, and mixed-vegetation linear equations) produce consistent evaluations of the vulnerability of the coastal marsh under high and low SLR rates. However, the *Spartina*-nonlinear scheme predicted the highest vegetation biomass and organic production rate, yielding the highest accretion rate and elevation, except for the mixed-veg case under the low SLR. The mixed-veg case represents the most resilient marsh type under low SLR with high K_b, but is the most vulnerable case under high SLR. Except the mixed-veg case under the low SLR, all the *Spartina*-linear cases predicted the largest marsh extent and smallest open water area.

The sensitivity analysis study identified the parameters whose values most critically affect model outcomes under different SLR conditions. The parametric sensitivity of the eco-geomorphologic models (e.g., the D- and M-model used in this study) were not the same under the high and low SLR conditions. For example, the most sensitive parameter, such as the maximum organic production rate, in the simulation under the high SLR, was not the most sensitive parameter in the low SLR scenario. The differences in parametric sensitivity highlighted the importance of evaluating parametric sensitivity under different external drivers.

The identified most sensitive parameters can help inform how to appropriately model key processes in different coastal marsh landscapes under SLR and vegetation evolution. These

This article is protected by copyright. All rights reserved.

identified key parameters under different climate change conditions can also serve to inform future field measurements studies.

Acknowledgments

We thank the constructive comments from Dr. Matthew Kirwan and the other two anonymous reviewers. The research presented in this paper was supported by the Laboratory Direct Research and Development program at Los Alamos National Laboratory under project number 20180033DR. This research used resources provided by the Los Alamos National Laboratory Institutional Computing Program, which is supported by the U.S. Department of Energy National Nuclear Security Administration under Contract No. 89233218CNA000001. MM and AD acknowledge support by Provveditorato for the Public Works of Veneto, Trentino Alto Adige, and Friuli Venezia Giulia, provided through the concessionary of State Consorzio Venezia Nuova and coordinated by CORILA in the framework of the Venezia 2021 Research Program

This study is a model-based study that uses two numerical models and synthetic experiments. The model source code are available in the model repositories from the Community Surface Dynamics Modeling System (CSDMS) https://csdms.colorado.edu/wiki/Model_download_portal. Model parameters are listed in the tables above.

References

Allen, J. R. (1995). Salt-marsh growth and fluctuating sea level: implications of a simulation model for Flandrian coastal stratigraphy and peat-based sea-level curves. *Sedimentary Geology*, *100*(1–4), 21–45.

Allen, J. R. (2000). Morphodynamics of Holocene salt marshes: a review sketch from the Atlantic and Southern North Sea coasts of Europe. *Quaternary Science Reviews*, *19*(12), 1155–1231.

This article is protected by copyright. All rights reserved.

Accepted Article

Accepted Article

Barbier, E. B., Hacker, S. D., Kennedy, C., Koch, E. W., Stier, A. C., & Silliman, B. R. (2011). The value of estuarine and coastal ecosystem services. *Ecological Monographs*, *81*(2), 169–193. https://doi.org/10.1890/10-1510.1

Belliard, J.-P., Toffolon, M., Carniello, L., & D'Alpaos, A. (2015). An ecogeomorphic model of tidal channel initiation and elaboration in progressive marsh accretional contexts. *Journal of Geophysical Research: Earth Surface*, *120*(6), 1040–1064. https://doi.org/10.1002/2015JF003445

Belliard, J.-P., Di Marco, N., Carniello, L., & Toffolon, M. (2016). Sediment and vegetation spatial dynamics facing sea-level rise in microtidal salt marshes: Insights from an ecogeomorphic model. *Advances in Water Resources*, *93*, 249–264. https://doi.org/10.1016/j.advwatres.2015.11.020

Best, Ü. S. N., Van der Wegen, M., Dijkstra, J., Willemsen, P. W. J. M., Borsje, B. W., & Roelvink, D. J. A. (2018). Do salt marshes survive sea level rise? Modelling wave action, morphodynamics and vegetation dynamics. *Environmental Modelling & Software*, *109*, 152–166. https://doi.org/10.1016/j.envsoft.2018.08.004

Brush Jr., L. M. (2012). Exploratory study of sediment diffusion. *Journal of Geophysical Research (1896-1977)*, 1427–1433. https://doi.org/10.1029/JZ067i004p01427@10.1002/(ISSN)2156-2202.EROSIO1

Burkett, V., & Kusler, J. (2000). CLIMATE CHANGE: POTENTIAL IMPACTS AND INTERACTIONS IN WETLANDS OF THE UNTTED STATES.

Cahoon, D. R., & Guntenspergen, G. R. (2010). Climate change, sea-level rise, and coastal wetlands. *National Wetlands Newsletter*, *32*(1), 8–12.

Cao, Z., Wolfram, P., Rowland, J., Zhang, Y., & Pasqualini, D. (2020). Estimating sediment settling velocities from a theoretically-guided, data-driven approach. *Journal of Hydraulic Engineering*. https://doi.org/10.1061/(ASCE)HY.1943-7900.0001798

Carniello, L., Defina, A., Fagherazzi, S., & D'Alpaos, L. (2005). A combined wind wave–tidal model for the Venice lagoon, Italy. *Journal of Geophysical Research: Earth Surface*, *110*(F4).

Carus, J., Paul, M., & Schröder, B. (2016). Vegetation as self-adaptive coastal protection: Reduction of current velocity and morphologic plasticity of a brackish marsh pioneer. *Ecology and Evolution*, *6*(6), 1579–1589. https://doi.org/10.1002/ece3.1904

Costanza, R., d'Arge, R., de Groot, R., Farber, S., Grasso, M., Hannon, B., et al. (1997). The value of the world's ecosystem services and natural capital. *Nature*, *387*(6630), 253–260. https://doi.org/10.1038/387253a0

This article is protected by copyright. All rights reserved.

Accepted Article

Cukier, R., Fortuin, C., Shuler, K. E., Petschek, A., & Schaibly, J. (1973). Study of the sensitivity of coupled reaction systems to uncertainties in rate coefficients. I Theory. *The Journal of Chemical Physics*, *59*(8), 3873–3878.

Da Lio, C., D'Alpaos, A., & Marani, M. (2013). The secret gardener: vegetation and the emergence of biogeomorphic patterns in tidal environments. *Philosophical Transactions of the Royal Society A: Mathematical, Physical and Engineering Sciences*, *371*(2004), 20120367.

D'Alpaos, A., & Marani, M. (2016). Reading the signatures of biologic–geomorphic feedbacks in salt-marsh landscapes. *Advances in Water Resources*, *93*, 265–275. https://doi.org/10.1016/j.advwatres.2015.09.004

D'Alpaos, A., Marani, M., & Rinaldo, A. (2007). Landscape evolution in tidal embayments: Modeling the interplay of erosion, sedimentation, and vegetation dynamics. *Journal of Geophysical Research: Earth Surface*, *112*(F1). https://doi.org/10.1029/2006JF000537

D'Alpaos, A., Mudd, S. M., & Carniello, L. (2011). Dynamic response of marshes to perturbations in suspended sediment concentrations and rates of relative sea level rise. *Journal of Geophysical Research: Earth Surface*, *116*(F4). https://doi.org/10.1029/2011JF002093

D'Alpaos, A., Lanzoni, S., Rinaldo, A., & Marani, M. (2019). Chapter 5 - Salt-Marsh Ecogeomorphological Dynamics and Hydrodynamic Circulation. In G. M. E. Perillo, E. Wolanski, D. R. Cahoon, & C. S. Hopkinson (Eds.), *Coastal Wetlands* (pp. 189–220). Elsevier. https://doi.org/10.1016/B978-0-444-63893-9.00005-8

Danielson, J. J., Poppenga, S. K., Brock, J. C., Evans, G. A., Tyler, D. J., Gesch, D. B., et al. (2016). Topobathymetric Elevation Model Development using a New Methodology: Coastal National Elevation Database. *Journal of Coastal Research*, *76*, 75–89. https://doi.org/10.2112/SI76-008

Day, J. W., Christian, R. R., Boesch, D. M., Yáñez-Arancibia, A., Morris, J., Twilley, R. R., et al. (2008). Consequences of climate change on the ecogeomorphology of coastal wetlands. *Estuaries and Coasts*, *31*(3), 477–491.

Duvall, M., Wiberg, P., & Kirwan, M. (2019). Controls on Sediment Suspension, Flux, and Marsh Deposition near a Bay-Marsh Boundary. *Estuaries and Coasts*, *42*(2), 403–424. https://doi.org/10.1007/s12237-018-0478-4

Fagherazzi, S. (2014). Storm-proofing with marshes. *Nature Geoscience*, *7*(10), 701–702. https://doi.org/10.1038/ngeo2262

This article is protected by copyright. All rights reserved.

Accepted Article

Fagherazzi, S., Kirwan, M., Mudd, S. M., Guntenspergen, G. R., Temmerman, S., D'Alpaos, A., et al. (2012). Numerical models of salt marsh evolution: Ecological, geomorphic, and climatic factors. *Reviews of Geophysics*, *50*(1).

FitzGerald, D. M., & Hughes, Z. (2019). Marsh Processes and Their Response to Climate Change and Sea-Level Rise. *Annual Review of Earth and Planetary Sciences*, *47*(1), 481–517. https://doi.org/10.1146/annurev-earth-082517-010255

French. (1993). Numerical simulation of vertical marsh growth and adjustment to accelerated sea-level rise, North Norfolk, UK. *Earth Surface Processes and Landforms*, *18*(1), 63–81.

French. (2006). Tidal marsh sedimentation and resilience to environmental change: Exploratory modelling of tidal, sea-level and sediment supply forcing in predominantly allochthonous systems. *Marine Geology*, *235*(1), 119–136. https://doi.org/10.1016/j.margeo.2006.10.009

Friedrichs, C. T., & Perry, J. E. (2001). Tidal Salt Marsh Morphodynamics: A Synthesis. *Journal of Coastal Research*, 7–37.

Ganju, N. K., Defne, Z., Kirwan, M. L., Fagherazzi, S., D'Alpaos, A., & Carniello, L. (2017). Spatially integrative metrics reveal hidden vulnerability of microtidal salt marshes. *Nature Communications*, *8*(1), 14156. https://doi.org/10.1038/ncomms14156

Ganju, N. K., Defne, Z., & Fagherazzi, S. (2020). Are Elevation and Open-Water Conversion of Salt Marshes Connected? *Geophysical Research Letters*, *47*(3), e2019GL086703. https://doi.org/10.1029/2019GL086703

Ghisalberti, M., & Nepf, H. (2005). Mass transport in vegetated shear flows. *Environmental Fluid Mechanics*, *5*(6), 527–551.

Gleichauf, K. T., Wolfram, P. J., Monsen, N. E., Fringer, O. B., & Monismith, S. G. (2014). Dispersion mechanisms of a tidal river junction in the Sacramento–San Joaquin Delta, California. *San Francisco Estuary and Watershed Science*, *12*(LA-UR-14-29557).

Hayhoe, K., Edmonds, J., Kopp, R., LeGrande, A., Sanderson, B., Wehner, M., & Wuebbles, D. (2017). *Climate models, scenarios, and projections* (Climate Science Special Report: Fourth National Climate Assessment No. Chapter 4) (p. 45). Washington, DC, USA: U.S. Global Change Research Program.

This article is protected by copyright. All rights reserved.

Accepted Article

Kirwan, M., & Blum, L. (2011). Enhanced decomposition offsets enhanced productivity and soil carbon accumulation in coastal wetlands responding to climate change. *Biogeosciences*, *8*(4), 987–993. https://doi.org/10.5194/bg-8-987-2011

Kirwan, M., & Murray, A. B. (2007). A coupled geomorphic and ecological model of tidal marsh evolution. *Proceedings of the National Academy of Sciences*, *104*(15), 6118–6122. https://doi.org/10.1073/pnas.0700958104

Kirwan, M., & Temmerman, S. (2009). Coastal marsh response to historical and future sea-level acceleration. *Quaternary Science Reviews*, *28*(17), 1801–1808. https://doi.org/10.1016/j.quascirev.2009.02.022

Kirwan, M., Murray, A. B., & Boyd, W. S. (2008). Temporary vegetation disturbance as an explanation for permanent loss of tidal wetlands. *Geophysical Research Letters*, *35*(5). https://doi.org/10.1029/2007GL032681

Kirwan, M., Guntenspergen, G. R., D'Alpaos, A., Morris, J. T., Mudd, S. M., & Temmerman, S. (2010). Limits on the adaptability of coastal marshes to rising sea level. *Geophysical Research Letters*, *37*(23). https://doi.org/10.1029/2010GL045489

Kirwan, M., Temmerman, S., Skeehan, E. E., Guntenspergen, G. R., & Fagherazzi, S. (2016). Overestimation of marsh vulnerability to sea level rise. *Nature Climate Change*, *6*(3), 253–260. https://doi.org/10.1038/nclimate2909

Kirwan, M., Walters, D. C., Reay, W. G., & Carr, J. A. (2016). Sea level driven marsh expansion in a coupled model of marsh erosion and migration. *Geophysical Research Letters*, *43*(9), 4366–4373. https://doi.org/10.1002/2016GL068507

Krone, R. B. (1962). Flume studies of transport of sediment in estrarial shoaling processes. *Final Report, Hydr.Engr.and Samitary Engr.Res.Lab., Univ.of California*. Retrieved from https://ci.nii.ac.jp/naid/10004496634/

Langley, J. A., McKee, K. L., Cahoon, D. R., Cherry, J. A., & Megonigal, J. P. (2009). Elevated CO2 stimulates marsh elevation gain, counterbalancing sea-level rise. *Proceedings of the National Academy of Sciences*, *106*(15), 6182–6186.

This article is protected by copyright. All rights reserved.

Accepted Article

Langston, A. K., Vinent, O. D., Herbert, E. R., & Kirwan, M. L. (2020). Modeling long-term salt marsh response to sea level rise in the sediment-deficient Plum Island Estuary, MA. *Limnology and Oceanography*, *9999*(n/a), 1–16. https://doi.org/10.1002/lno.11444

Lesser, G., Roelvink, J., Van Kester, J., & Stelling, G. (2004). Development and validation of a three-dimensional morphological model. *Coastal Engineering*, *51*(8), 883–915.

Marani, M., Lanzoni, S., Silvestri, S., & Rinaldo, A. (2004). Tidal landforms, patterns of halophytic vegetation and the fate of the lagoon of Venice. *Journal of Marine Systems*, *51*(1), 191–210. https://doi.org/10.1016/j.jmarsys.2004.05.012

Marani, M., D'Alpaos, A., Lanzoni, S., Carniello, L., & Rinaldo, A. (2007). Biologically□controlled multiple equilibria of tidal landforms and the fate of the Venice lagoon. *Geophysical Research Letters*, *34*(11).

Marani, M., D'Alpaos, A., Lanzoni, S., Carniello, L., & Rinaldo, A. (2010). The importance of being coupled: Stable states and catastrophic shifts in tidal biomorphodynamics. *Journal of Geophysical Research: Earth Surface*, *115*(F4).

Marani, M., Da Lio, C., & D'Alpaos, A. (2013). Vegetation engineers marsh morphology through multiple competing stable states. *Proceedings of the National Academy of Sciences*, *110*(9), 3259–3263.

Mariotti, G. (2016). Revisiting salt marsh resilience to sea level rise: Are ponds responsible for permanent land loss? *Journal of Geophysical Research: Earth Surface*, *121*(7), 1391–1407. https://doi.org/10.1002/2016JF003900

Mariotti, G., & Fagherazzi, S. (2010). A numerical model for the coupled long-term evolution of salt marshes and tidal flats. *Journal of Geophysical Research: Earth Surface*, *115*(F1). https://doi.org/10.1029/2009JF001326

Moller, I., Kudella, M., Rupprecht, F., Spencer, T., Paul, M., van Wesenbeeck, B. K., et al. (2014). Wave attenuation over coastal salt marshes under storm surge conditions. *Nature Geoscience*, *7*(10), 727–731. https://doi.org/10.1038/ngeo2251

Morris, J. T. (2006). Competition among marsh macrophytes by means of geomorphological displacement in the intertidal zone. *Estuarine, Coastal and Shelf Science*, *69*(3–4), 395–402.

This article is protected by copyright. All rights reserved.

Accepted Article

Morris, J. T., & Bowden, W. B. (1986). A Mechanistic, Numerical Model of Sedimentation, Mineralization, and Decomposition for Marsh Sediments. *Soil Science Society of America Journal*, *50*(1), 96–105. https://doi.org/10.2136/sssaj1986.03615995005000010019x

Morris, J. T., Sundareshwar, P., Nietch, C. T., Kjerfve, B., & Cahoon, D. R. (2002). Responses of coastal wetlands to rising sea level. *Ecology*, *83*(10), 2869–2877.

Morris, J. T., Barber, D. C., Callaway, J. C., Chambers, R., Hagen, S. C., Hopkinson, C. S., et al. (2016). Contributions of organic and inorganic matter to sediment volume and accretion in tidal wetlands at steady state. *Earth's Future*, *4*(4), 110–121. https://doi.org/10.1002/2015EF000334

Mudd, S. M., Fagherazzi, S., Morris, J. T., & Furbish, D. J. (2004). Flow, sedimentation, and biomass production on a vegetated salt marsh in South Carolina: toward a predictive model of marsh morphologic and ecologic evolution. *The Ecogeomorphology of Tidal Marshes, Coastal Estuarine Stud*, *59*, 165–187.

Mudd, S. M., Howell, S. M., & Morris, J. T. (2009). Impact of dynamic feedbacks between sedimentation, sea-level rise, and biomass production on near-surface marsh stratigraphy and carbon accumulation. *Estuarine, Coastal and Shelf Science*, *82*(3), 377–389.

Mudd, S. M., D'Alpaos, A., & Morris, J. T. (2010). How does vegetation affect sedimentation on tidal marshes? Investigating particle capture and hydrodynamic controls on biologically mediated sedimentation. *Journal of Geophysical Research: Earth Surface*, *115*(F3). https://doi.org/10.1029/2009JF001566

National Ocean Service. (2018, August 13). Where is the highest tide? Retrieved from https://oceanservice.noaa.gov/facts/highesttide.html#26

Nepf, H. (1999). Drag, turbulence, and diffusion in flow through emergent vegetation. *Water Resources Research*, *35*(2), 479–489.

NOAA. (2001). NOAA tide and water level: Cape May, NJ, Station ID:8536110. Retrieved from https://tidesandcurrents.noaa.gov/stationhome.html?id=8536110

Orson, R., Panageotou, W., & Leatherman, S. P. (1985). Response of tidal salt marshes of the US Atlantic and Gulf coasts to rising sea levels. *Journal of Coastal Research*, 29–37.

Palinkas, C. M., & Engelhardt, K. A. M. (2019). Influence of Inundation and Suspended-Sediment Concentrations on Spatiotemporal Sedimentation Patterns in a Tidal Freshwater Marsh. *Wetlands*, *39*(3), 507–520. https://doi.org/10.1007/s13157-018-1097-3

This article is protected by copyright. All rights reserved.

Accepted Article

Palmer, M. R., Nepf, H. M., Pettersson, T. J. R., & Ackerman, J. D. (2004). Observations of particle capture on a cylindrical collector: Implications for particle accumulation and removal in aquatic systems. *Limnology and Oceanography*, *49*(1), 76–85. https://doi.org/10.4319/lo.2004.49.1.0076

Parchure Trimbak M., & Mehta Ashish J. (1985). Erosion of Soft Cohesive Sediment Deposits. *Journal of Hydraulic Engineering*, *111*(10), 1308–1326. https://doi.org/10.1061/(ASCE)0733-9429(1985)111:10(1308)

Randerson, P. (1979). A simulation model of salt-marsh development and plant ecology. *Estuarine and Coastal Land Reclamation and Water Storage*, 48–67.

Ratliff, K. M., Braswell, A. E., & Marani, M. (2015). Spatial response of coastal marshes to increased atmospheric CO2. *Proceedings of the National Academy of Sciences*, *112*(51), 15580–15584. https://doi.org/10.1073/pnas.1516286112

Reed, D. J. (1995). The response of coastal marshes to sea-level rise: Survival or submergence? *Earth Surface Processes and Landforms*, *20*(1), 39–48.

Riazi, A., & Türker, U. (2019). The drag coefficient and settling velocity of natural sediment particles. *Computational Particle Mechanics*, *6*(3), 427–437. https://doi.org/10.1007/s40571-019-00223-6

Rinaldo, A., Fagherazzi, S., Lanzoni, S., Marani, M., & Dietrich, W. E. (1999). Tidal networks: 2. Watershed delineation and comparative network morphology. *Water Resources Research*, *35*(12), 3905–3917. https://doi.org/10.1029/1999wr900237

Roelvink, J. (2006). Coastal morphodynamic evolution techniques. *Coastal Engineering*, *53*(2), 277–287.

Rogers, K., Saintilan, N., & Copeland, C. (2012). Modelling wetland surface elevation dynamics and its application to forecasting the effects of sea-level rise on estuarine wetlands. *Ecological Modelling*, *244*, 148–157. https://doi.org/10.1016/j.ecolmodel.2012.06.014

Roner, M., D'Alpaos, A., Ghinassi, M., Marani, M., Silvestri, S., Franceschinis, E., & Realdon, N. (2016). Spatial variation of salt-marsh organic and inorganic deposition and organic carbon accumulation: Inferences from the Venice lagoon, Italy. *Advances in Water Resources*, *93*, 276–287. https://doi.org/10.1016/j.advwatres.2015.11.011

Roulet, N. (1990). The hydrological role of peat□covered wetlands. *The Canadian Geographer/Le Géographe Canadien*, *34*(1), 82–83.

This article is protected by copyright. All rights reserved.

Accepted Article

Scavia, D., Field, J. C., Boesch, D. F., Buddemeier, R. W., Burkett, V., Cayan, D. R., et al. (2002). Climate change impacts on U.S. Coastal and Marine Ecosystems. *Estuaries*, *25*(2), 149–164. https://doi.org/10.1007/BF02691304

Scheidegger, A. (1961). Mathematical models of slope development. *Geological Society of America Bulletin*, *72*(1), 37–50.

Schepers, L., Kirwan, M., Guntenspergen, G., & Temmerman, S. (2017). Spatio-temporal development of vegetation die-off in a submerging coastal marsh. *Limnology and Oceanography*, *62*(1), 137–150. https://doi.org/10.1002/lno.10381

Schile, L. M., Callaway, J. C., Morris, J. T., Stralberg, D., Parker, V. T., & Kelly, M. (2014). Modeling Tidal Marsh Distribution with Sea-Level Rise: Evaluating the Role of Vegetation, Sediment, and Upland Habitat in Marsh Resiliency. *PLOS ONE*, *9*(2), e88760. https://doi.org/10.1371/journal.pone.0088760

Schuerch, M., Spencer, T., Temmerman, S., Kirwan, M., Wolff, C., Lincke, D., et al. (2018). Future response of global coastal wetlands to sea-level rise. *Nature*, *561*(7722), 231–234. https://doi.org/10.1038/s41586-018-0476-5

Schwarz, C., Gourgue, O., van Belzen, J., Zhu, Z., Bouma, T. J., van de Koppel, J., et al. (2018). Self-organization of a biogeomorphic landscape controlled by plant life-history traits. *Nature Geoscience*, *11*(9), 672–677. https://doi.org/10.1038/s41561-018-0180-y

Silvestri, S., & Marani, M. (2004). Salt-marsh vegetation and morphology: Basic physiology, modelling and remote sensing observations. *The Ecogeomorphology of Tidal Marshes, Coastal Estuarine Stud*, *59*, 5–25.

Silvestri, S., Defina, A., & Marani, M. (2005). Tidal regime, salinity and salt marsh plant zonation. *Estuarine, Coastal and Shelf Science*, *62*(1), 119–130. https://doi.org/10.1016/j.ecss.2004.08.010

Song, X., Zhang, J., Zhan, C., Xuan, Y., Ye, M., & Xu, C. (2015). Global sensitivity analysis in hydrological modeling: Review of concepts, methods, theoretical framework, and applications. *Journal of Hydrology*, *523*, 739–757.

Spencer, T., Schuerch, M., Nicholls, R. J., Hinkel, J., Lincke, D., Vafeidis, A. T., et al. (2016). Global coastal wetland change under sea-level rise and related stresses: The DIVA Wetland Change Model. *Global and Planetary Change*, *139*, 15–30. https://doi.org/10.1016/j.gloplacha.2015.12.018

This article is protected by copyright. All rights reserved.

Accepted Article

Stralberg, D., Brennan, M., Callaway, J. C., Wood, J. K., Schile, L. M., Jongsomjit, D., et al. (2011). Evaluating Tidal Marsh Sustainability in the Face of Sea-Level Rise: A Hybrid Modeling Approach Applied to San Francisco Bay. *PLOS ONE*, *6*(11), e27388. https://doi.org/10.1371/journal.pone.0027388

Stumpf, R. P. (1983). The process of sedimentation on the surface of a salt marsh. *Estuarine, Coastal and Shelf Science*, *17*(5), 495–508.

Temmerman, S., Govers, G., Meire, P., & Wartel, S. (2003). Modelling long-term tidal marsh growth under changing tidal conditions and suspended sediment concentrations, Scheldt estuary, Belgium. *Marine Geology*, *193*(1), 151–169. https://doi.org/10.1016/S0025-3227(02)00642-4

Temmerman, S., Bouma, T. J., Govers, G., Wang, Z. B., Vries, M. B. D., & Herman, P. M. J. (2005). Impact of vegetation on flow routing and sedimentation patterns: Three-dimensional modeling for a tidal marsh. *Journal of Geophysical Research: Earth Surface*, *110*(F4). https://doi.org/10.1029/2005JF000301

Thompson, C. E. L., Amos, C. L., & Umgiesser, G. (2004). A comparison between fluid shear stress reduction by halophytic plants in Venice Lagoon, Italy and Rustico Bay, Canada—analyses of in situ measurements. *Journal of Marine Systems*, *51*(1), 293–308. https://doi.org/10.1016/j.jmarsys.2004.05.017

Thorne, K., MacDonald, G., Guntenspergen, G., Ambrose, R., Buffington, K., Dugger, B., et al. (2018). U.S. Pacific coastal wetland resilience and vulnerability to sea-level rise. *Science Advances*, *4*(2), eaao3270. https://doi.org/10.1126/sciadv.aao3270

Tiner, R. W. (2013). *Tidal Wetlands Primer*. University of Massachusetts Press.

Van Rijn, L. C. (1993). *Principles of sediment transport in rivers, estuaries and coastal seas* (Vol. 1006). Aqua publications Amsterdam.

Vreugdenhil, C. B. (2013). *Numerical methods for shallow-water flow* (Vol. 13). Springer Science & Business Media.

van Wijnen, H. J., & Bakker, J. P. (2001). Long-term Surface Elevation Change in Salt Marshes: a Prediction of Marsh Response to Future Sea-Level Rise. *Estuarine, Coastal and Shelf Science*, *52*(3), 381–390. https://doi.org/10.1006/ecss.2000.0744

Wohl, E., Brierley, G., Cadol, D., Coulthard, T. J., Covino, T., Fryirs, K. A., et al. (2019). Connectivity as an emergent property of geomorphic systems. *Earth Surface Processes and Landforms*, *44*(1), 4–26.

This article is protected by copyright. All rights reserved.

Accepted Article

Wolfram, P. J., Fringer, O. B., Monsen, N. E., Gleichauf, K. T., Fong, D. A., & Monismith, S. G. (2016). Modeling intrajunction dispersion at a well-mixed tidal river junction. *Journal of Hydraulic Engineering*, *142*(8), 04016019.

Xu, C., & Gertner, G. (2011). Understanding and comparisons of different sampling approaches for the Fourier Amplitudes Sensitivity Test (FAST). *Computational Statistics & Data Analysis*, *55*(1), 184–198.

Xu, C., & Gertner, G. Z. (2008a). A general first-order global sensitivity analysis method. *Reliability Engineering & System Safety*, *93*(7), 1060–1071.

Xu, C., & Gertner, G. Z. (2008b). Uncertainty and sensitivity analysis for models with correlated parameters. *Reliability Engineering & System Safety*, *93*(10), 1563–1573.

Yang, S. L., Shi, B. W., Bouma, T. J., Ysebaert, T., & Luo, X. X. (2012). Wave Attenuation at a Salt Marsh Margin: A Case Study of an Exposed Coast on the Yangtze Estuary. *Estuaries and Coasts*, *35*(1), 169–182. https://doi.org/10.1007/s12237-011-9424-4

Yousefi Lalimi, F., Marani, M., Heffernan, J. B., D'Alpaos, A., & Murray, A. B. (2020). Watershed and ocean controls of salt marsh extent and resilience. *Earth Surface Processes and Landforms*, *n/a*(n/a). https://doi.org/10.1002/esp.4817

Zhang, Y., Slingerland, R., & Duffy, C. (2016). Fully-coupled hydrologic processes for modeling landscape evolution. *Environmental Modelling & Software*, *82*, 89–107.

Zhang, Y., Li, W., Sun, G., Miao, G., Noormets, A., Emanuel, R., & King, J. S. (2018). Understanding coastal wetland hydrology with a new regional scale process-based hydrologic model. *Hydrological Processes*. https://doi.org/10.1002/hyp.13247

Table 1. The numerical experiment cases for the individual simulations.

	Spartina-dominant linear function	**Spartina-dominant nonlinear function**	**Mixed species linear function**
High SLR rate (0.01 m/yr) and High K_b (0.005 m/yr)	Case 1	Case 2	Case 3

This article is protected by copyright. All rights reserved.

Low SLR rate (0.005 m/yr) and High K_b (0.005 m/yr)	Case 4	Case 5	Case 6
High SLR rate (0.01 m/yr) and Low K_b (0.003 m/yr)	Case 7	Case 8	Case 9
Low SLR rate (0.005 m/yr) and Low K_b (0.003 m/yr)	Case 10	Case 11	Case 12

Table 2. Key hydro-eco-geomorphic parameters used in the individual simulations and parameter ranges used for ensemble simulations in the sensitivity analysis.

Processes	**Parameter description**	**Symbol in the D model**	**Range**	**Individual simulation**	**References**
Erosion	Erosion coefficient ($\frac{kg}{m^2 s P_a}$)	α	[2.00E-09, 4.12E-04]	1.12E-04	(D'Alpaos et al., 2007; Mariotti & Fagherazzi, 2010)
	Critical shear stress for erosion (P_a)	τ_e	[0.03, 2]	0.4	(Thompson et al., 2004)
Sedimentation	Critical shear stress for deposition (P_a)	τ_d	[0.05, 2]	0.1	(Parchure Trimbak M. &

This article is protected by copyright. All rights reserved.

					Mehta Ashish J., 1985)
	Sediment concentration at seaward boundary ($\frac{\mathrm{mg}}{\mathrm{liter}}$)	C_0	[1, 800]	20	(Kirwan et al., 2010)
	Suspended sediment diffusivity ($\frac{\mathrm{m}^2}{\mathrm{s}}$)	Sed_{diff}	[0.005, 1]	0.3	(Brush Jr., 2012)
	Sediment settling velocity ($\frac{\mathrm{m}}{\mathrm{s}}$)	w_s	[5.00E-05, 6.00E-04]	1.00E-04	(Riazi & Türker, 2019)
	Belowground organic production ($\frac{\mathrm{m}}{\mathrm{yr}}$)	K_b	[0, 0.0135]	0.003 and 0.005	(Morris et al., 2016; Mudd et al., 2010; Ratliff et al., 2015)
Forcing	Tidal amplitude (m)	AmpTide	[0.1, 4]	0.8	(National Ocean Service, 2018)

Accepted Article

This article is protected by copyright. All rights reserved.

Accepted Article

Biomass	Minimum depth between MHTL and land surface (m)	D_{biomin}	[0, 0.1]	0.1	(Morris, 2006)
	Maximum depth between MHTL and land surface (m)	D_{biomax}	[0.8, 0.95]	0.8	(Morris, 2006)
	Maximum biomass $(\frac{g}{m^2})$	B_{max}	[0, 3000]	2000	(Mudd et al., 2004)
Hydro-dynamics	Chezy coefficient $(\frac{m^{0.5}}{s})$	CHI	10	10	(D'Alpaos et al., 2007)
	Maximum water velocity $(\frac{m}{s})$	U_{max}	0.2	0.2	(D'Alpaos et al., 2007)

This article is protected by copyright. All rights reserved.

Accepted Article

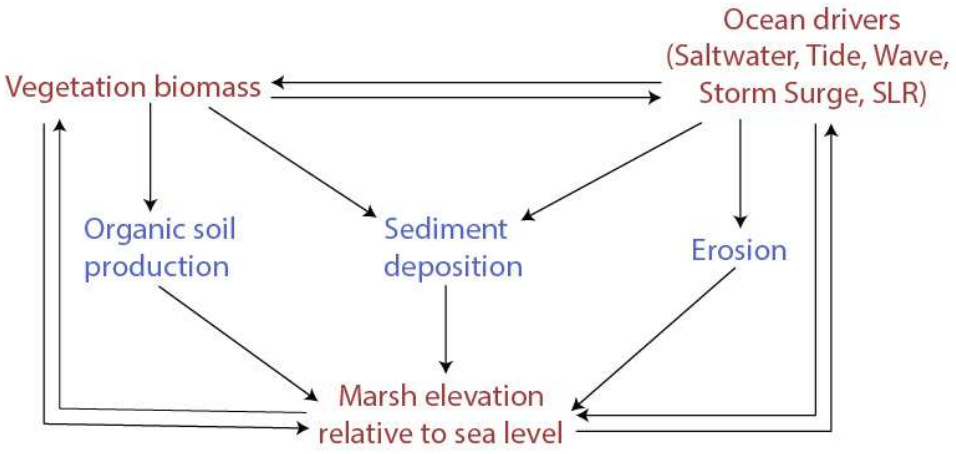

Figure 1. The linkage of hydro-ecogeomorphologic components in coastal marsh systems. The words in red and blue describe the components and sediment fluxes, respectively.

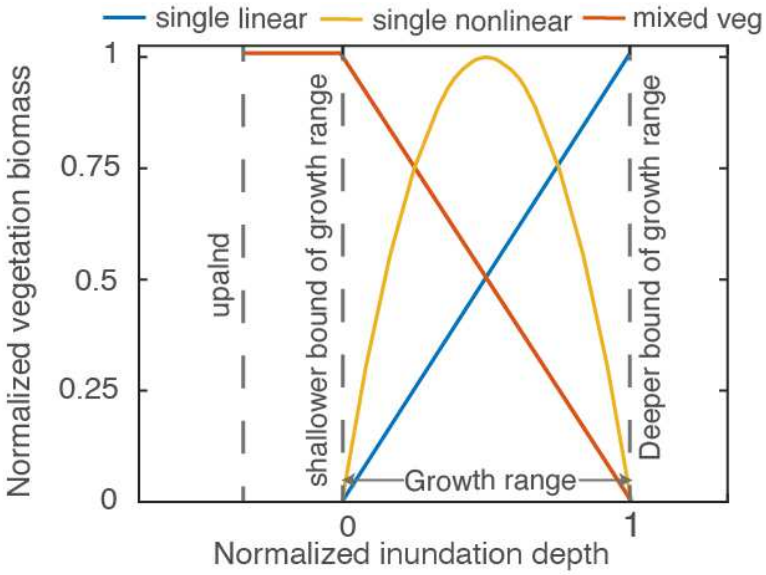

Figure 2 The dynamics of vegetation biomass under different marsh inundation depth normalized by the vegetation growth range bounded by $MHTL - D_{biomin}$ and $MHTL - D_{biomax}$. $MHTL$ represents the mean highest tide level. D_{biomax} and D_{biomin} are the highest and lowest inundation depth below MHTL, respectively.

This article is protected by copyright. All rights reserved.

Accepted Article

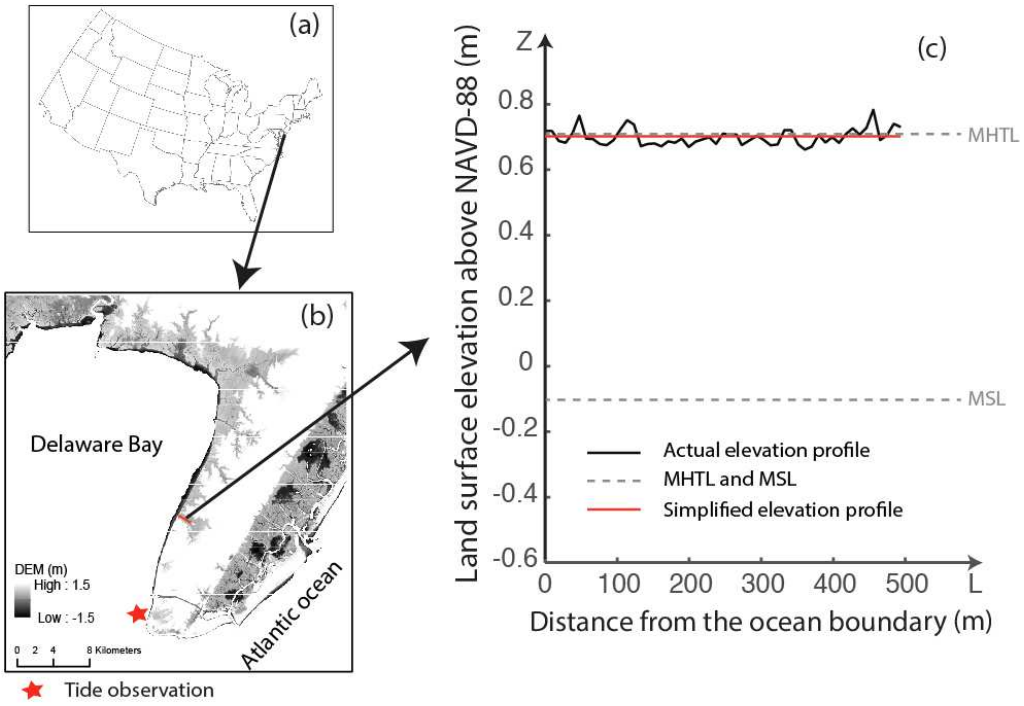

Figure 3 The geographic location and the elevation profile of a 1-D transect at Delaware Bay. (a) and (b) indicate the location of the 1-D transect. The black solid line in (c) shows the actual elevation profile of the 1-D transect. The red line is a simplified elevation profile. The gray dashed lines indicate the MHTL (mean highest tide level) and MSL (mean sea level)

This article is protected by copyright. All rights reserved.

Accepted Article

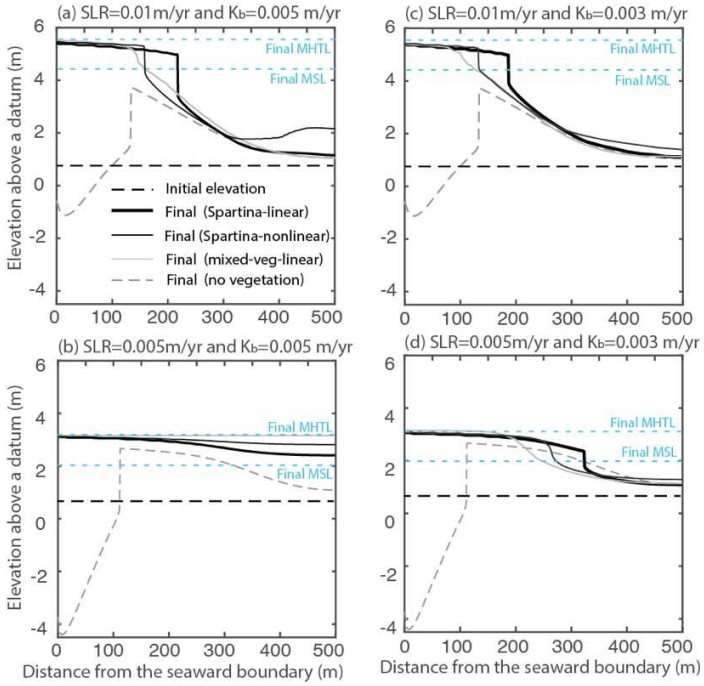

Figure 4. Elevation profiles after 500 years simulation by the D-model from the seaward boundary (x axis = 0 m) to the upland boundary (x axis = 500 m) for (a) the higher rate of SLR and higher K_b scenario, (b) the lower rate of SLR and higher K_b scenario, (c) the higher rate of SLR and lower K_b scenario, and (d) the lower rate of SLR and lower K_b scenario. The black dashed lines show the initial elevation profile (0.67 m above NAVD88 datum). The thicker and thinner black lines indicate the simulated elevation profiles by using Spartina dominant linear equation and Spartina dominant nonlinear equation, respectively. The gray solid lines are the elevation profiles by using the mixed vegetation linear equation. The gray dashed lines are the simulated elevation profiles without vegetation. The light blue dashed lines indicate the final MHTL and MSL.

This article is protected by copyright. All rights reserved.

Accepted Article

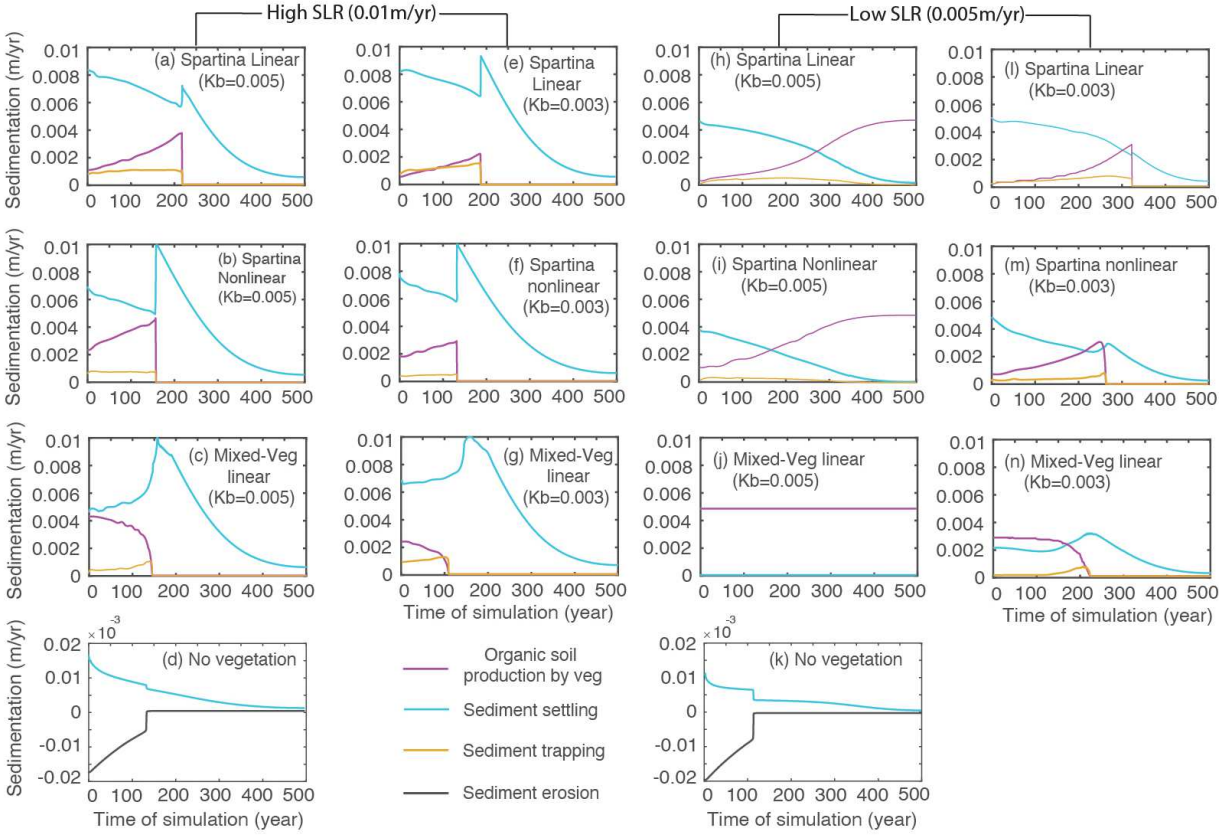

Figure 5. Spatial distribution of the sediment fluxes at the end of 500 years in the D-model simulations. The plots with various colors represent different fluxes in different scenarios.

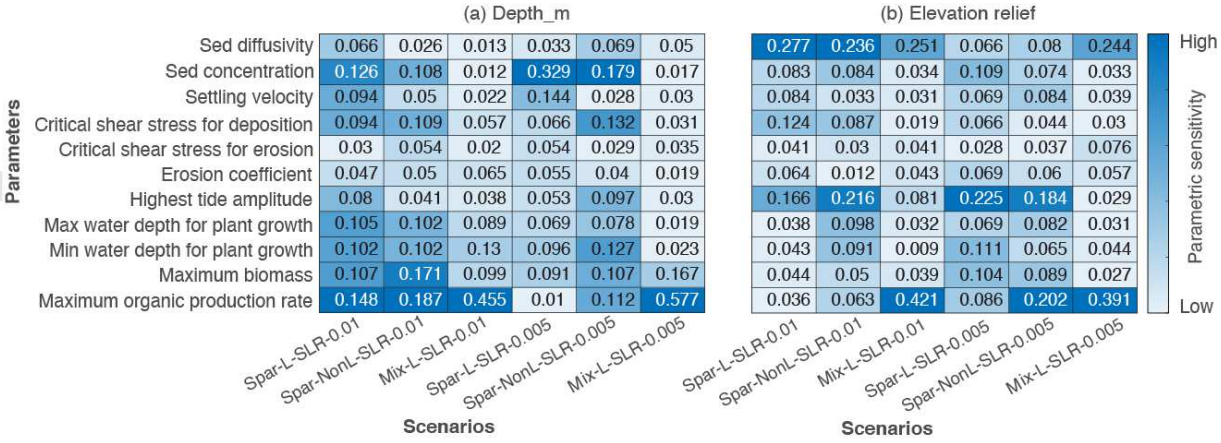

Figure 6. Parametric sensitivity of elevation change from the D-model simulations under (a) high SLR scenario and (b) low SLR scenario. The colors indicate model sensitivity with a high sensitivity coded in dark blue and low sensitivity coded in light blue. The values in each grid represents the sensitivity of the model to the corresponding parameter and simulation case.

This article is protected by copyright. All rights reserved.

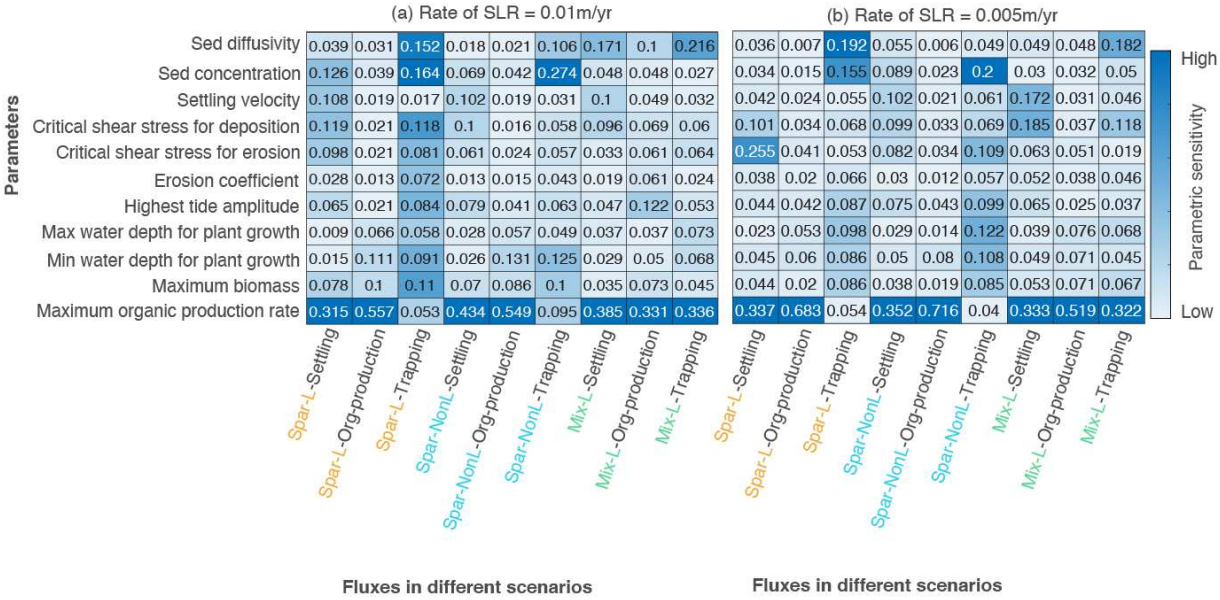

Figure 7. Parametric sensitivity of the sediment fluxes from the D-model simulations under (a) high SLR scenario and (b) low SLR scenario. The colors indicate model sensitivity with a high sensitivity coded in dark blue and low sensitivity coded in light blue. The value in each grid represents the sensitivity of the model to the corresponding parameter, flux, and simulation case.

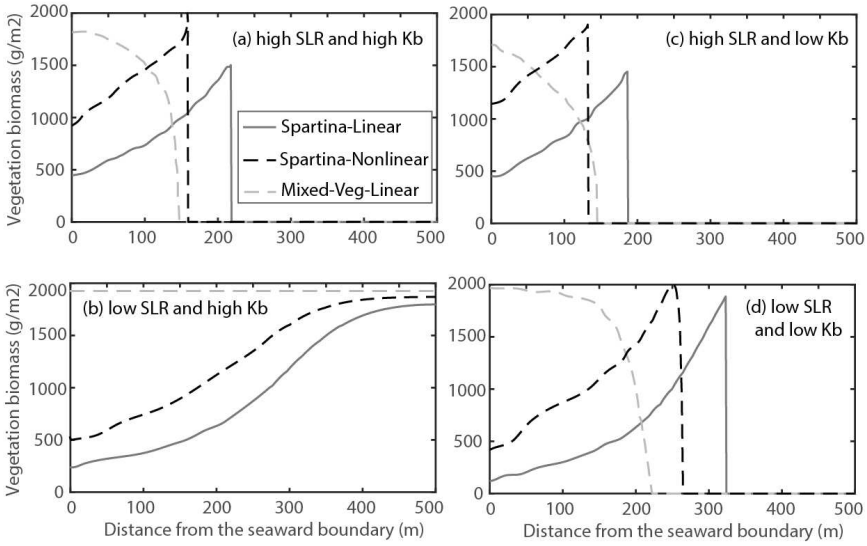

Figure 8. The spatial distribution of vegetation biomass from the D-model simulations at the end of 500 years throughout the marsh domain under (a) the high SLR and higher K_b scenario, (b) the low SLR and higher K_b scenario, (c) the higher SLR and lower K_b scenario, and (d) the lower SLR and lower K_b scenario.

This article is protected by copyright. All rights reserved.

Accepted Article

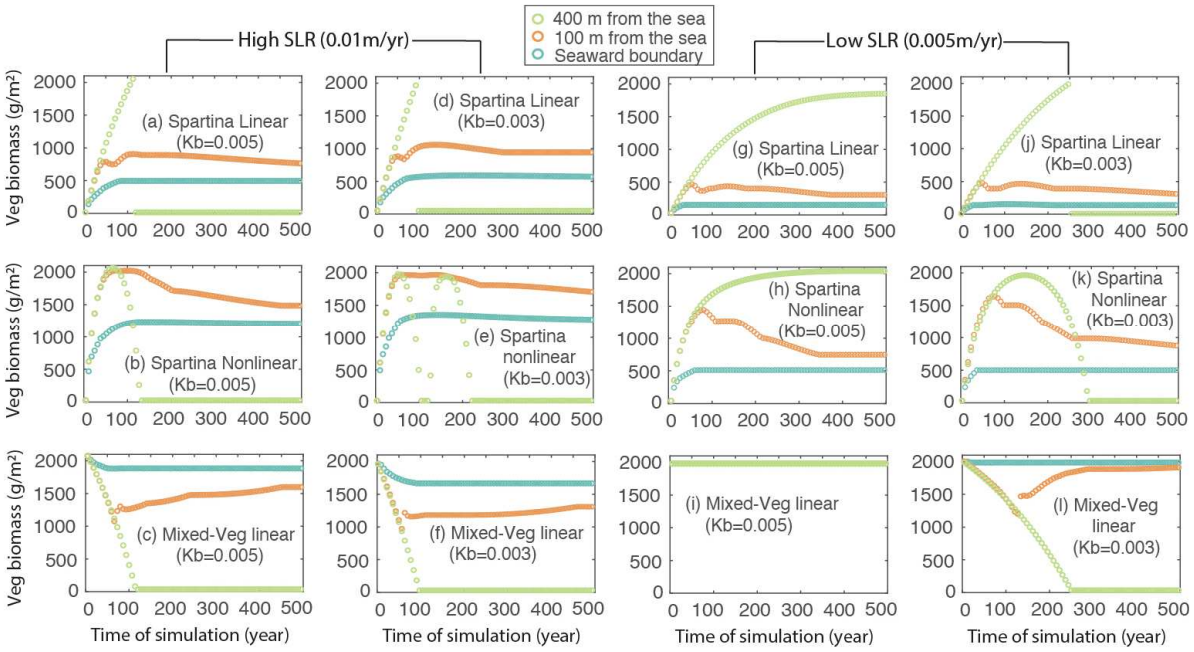

Figure 9. Temporal variation of vegetation biomass for different vegetation cases from the D-model simulations in different SLR scenarios. The circles in different colors indicate the biomass at different locations of the marsh domain.

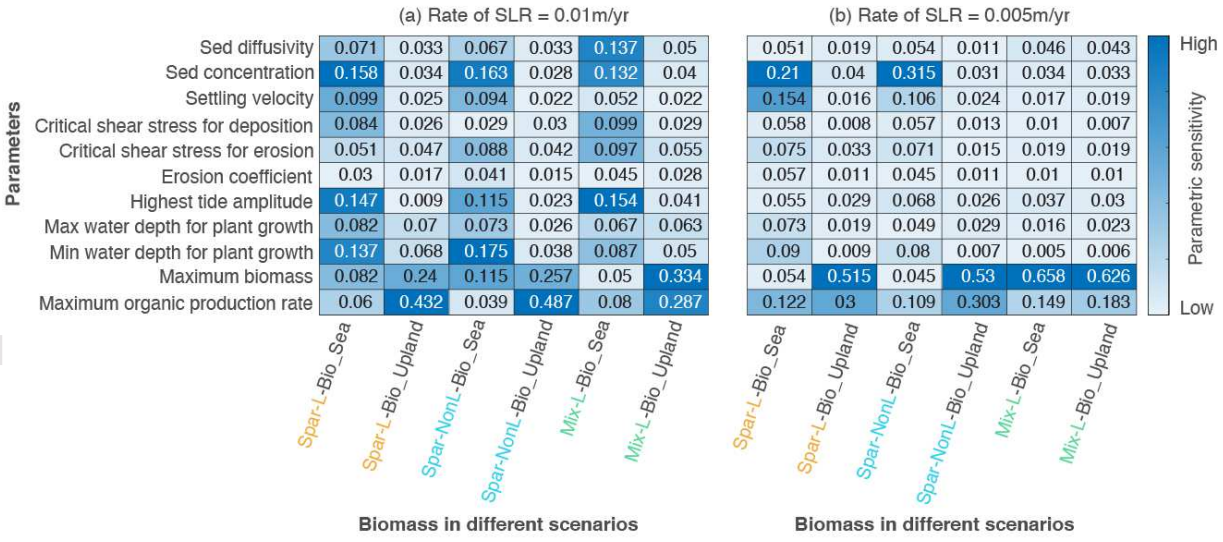

Figure 10. Parametric sensitivity of vegetation biomass from the D-model simulations under (a) high SLR scenario and (b) low SLR scenario. The colors indicate model sensitivity with a high sensitivity coded in dark blue and low sensitivity coded in light blue. The value in each grid represents the sensitivity of the model to the corresponding parameter, biomass, and simulation case.

This article is protected by copyright. All rights reserved.

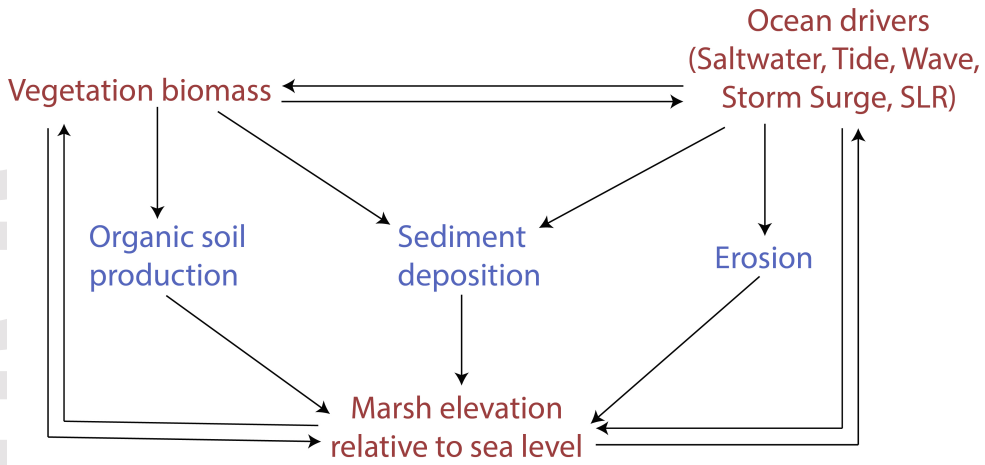

Accepted Article

This article is protected by copyright. All rights reserved.

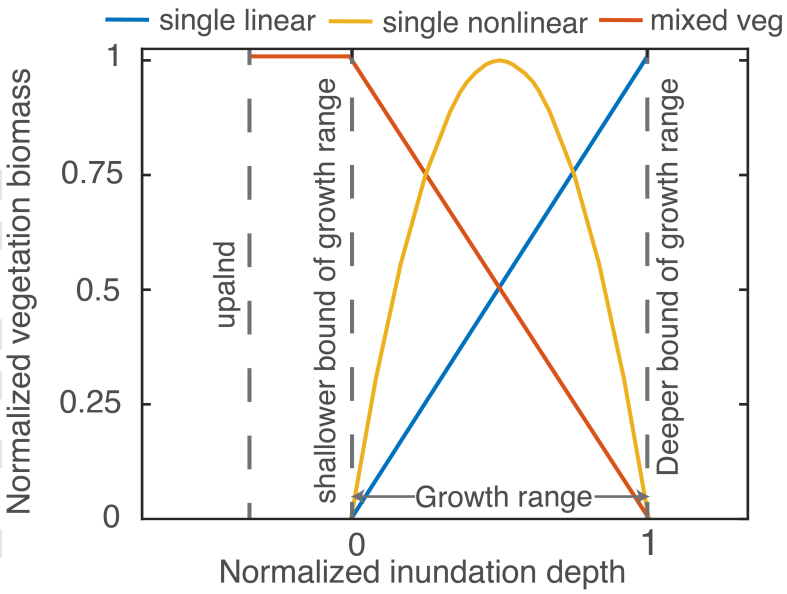

Accepted Article

This article is protected by copyright. All rights reserved.

Accepted Article

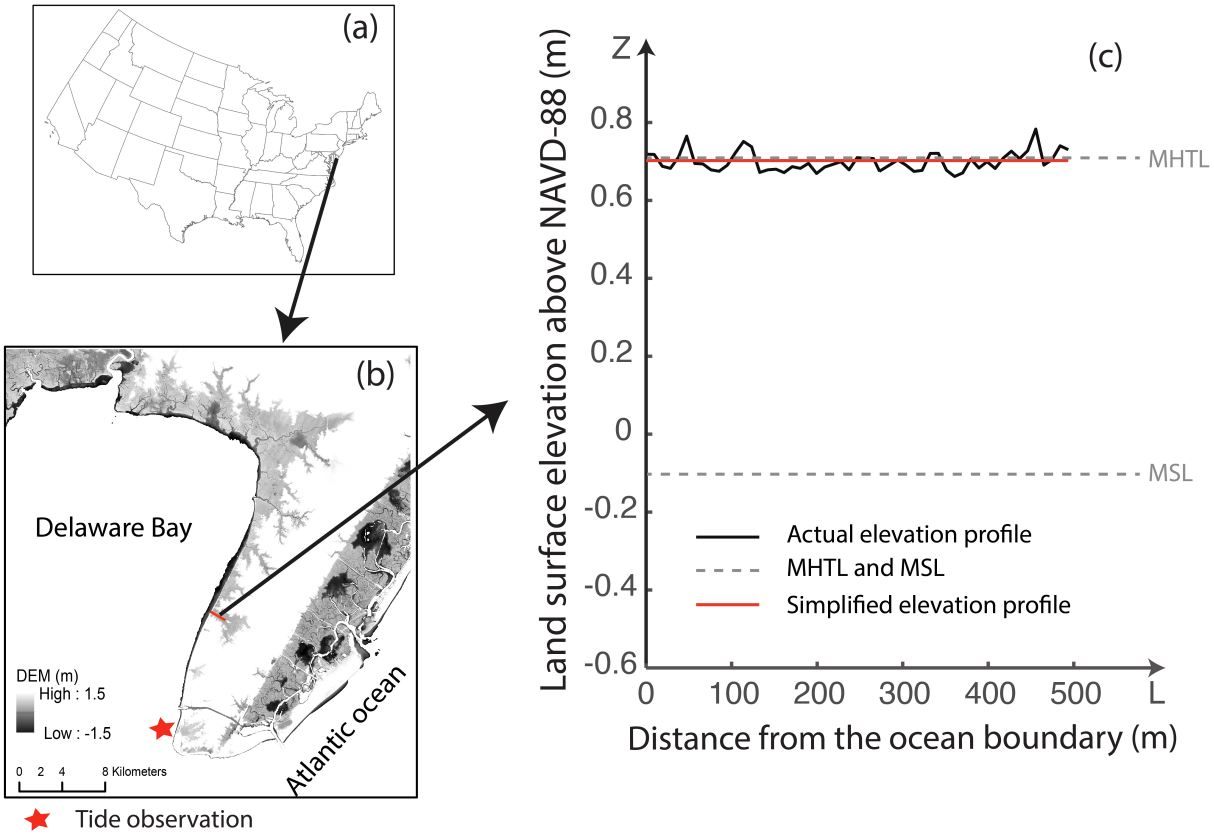

This article is protected by copyright. All rights reserved.

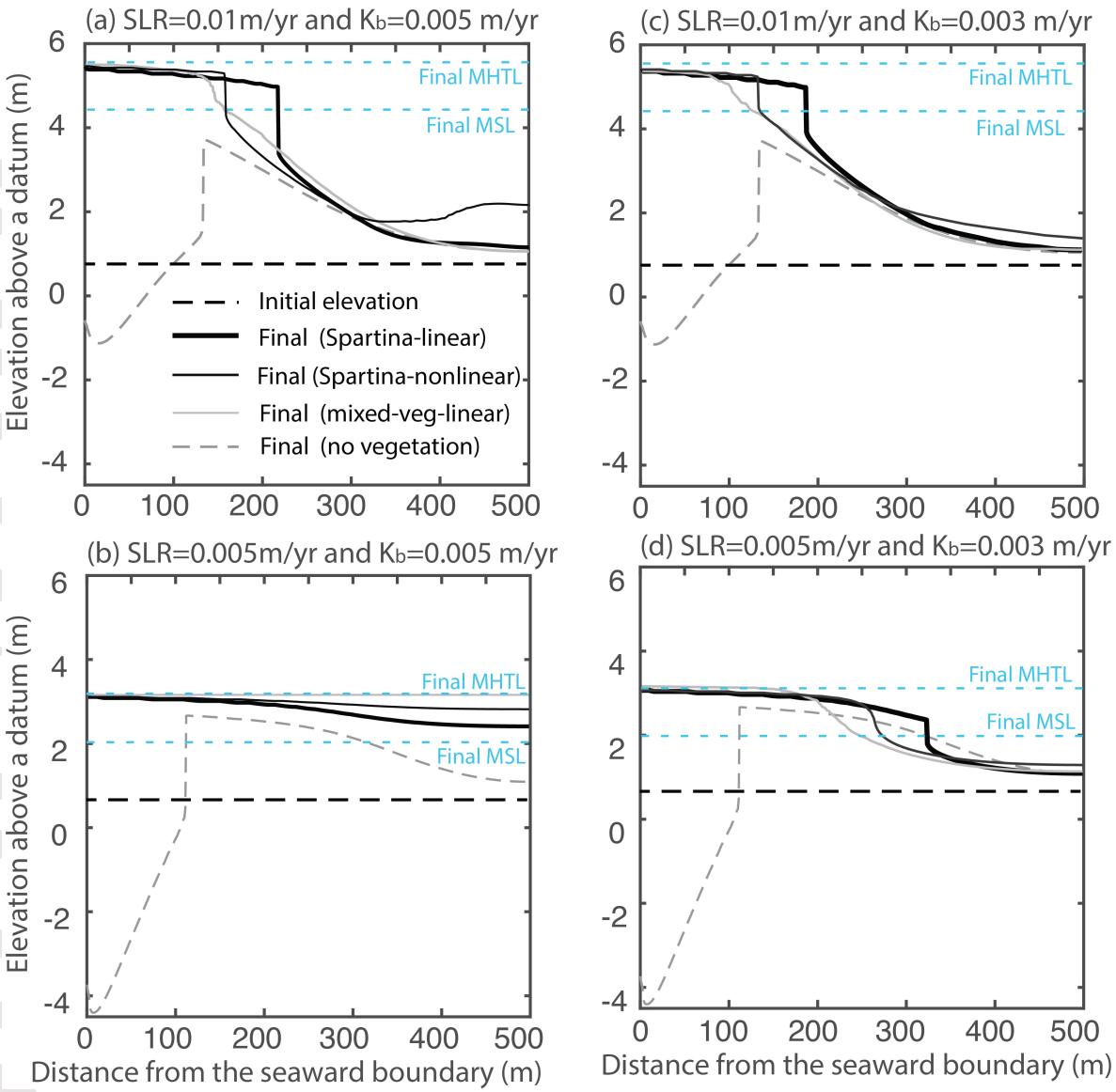

Accepted Article

This article is protected by copyright. All rights reserved.

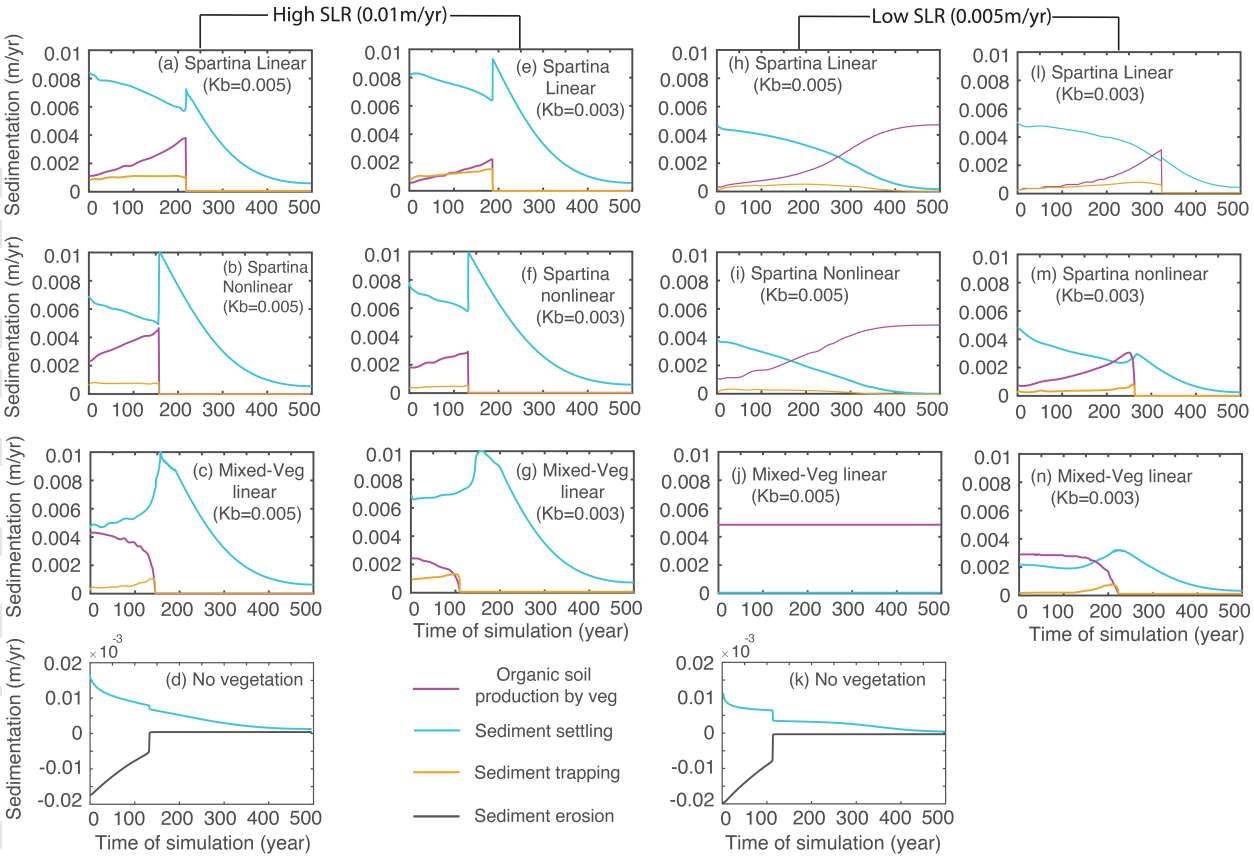

Accepted Article

This article is protected by copyright. All rights reserved.

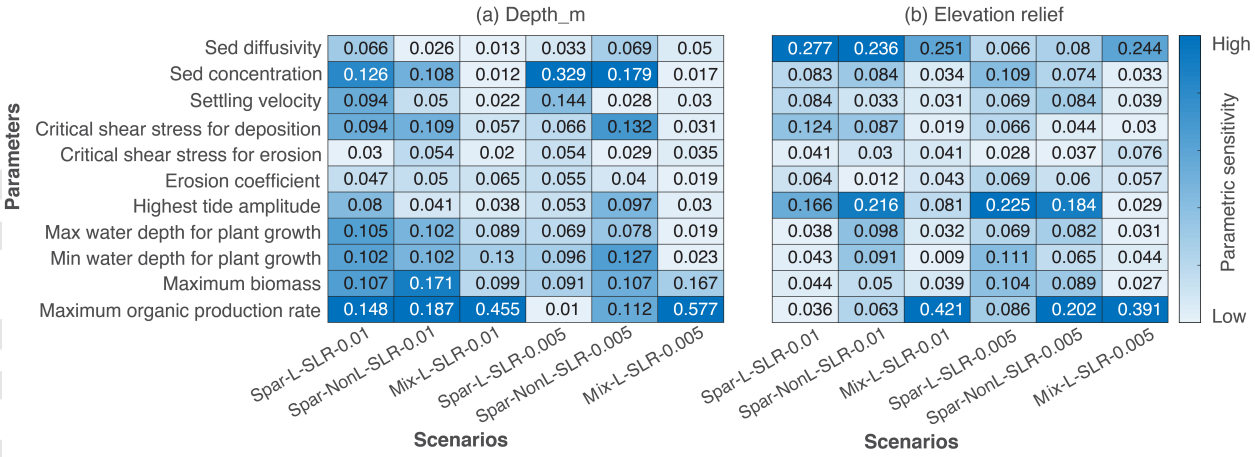

Accepted Article

This article is protected by copyright. All rights reserved.

Accepted Article

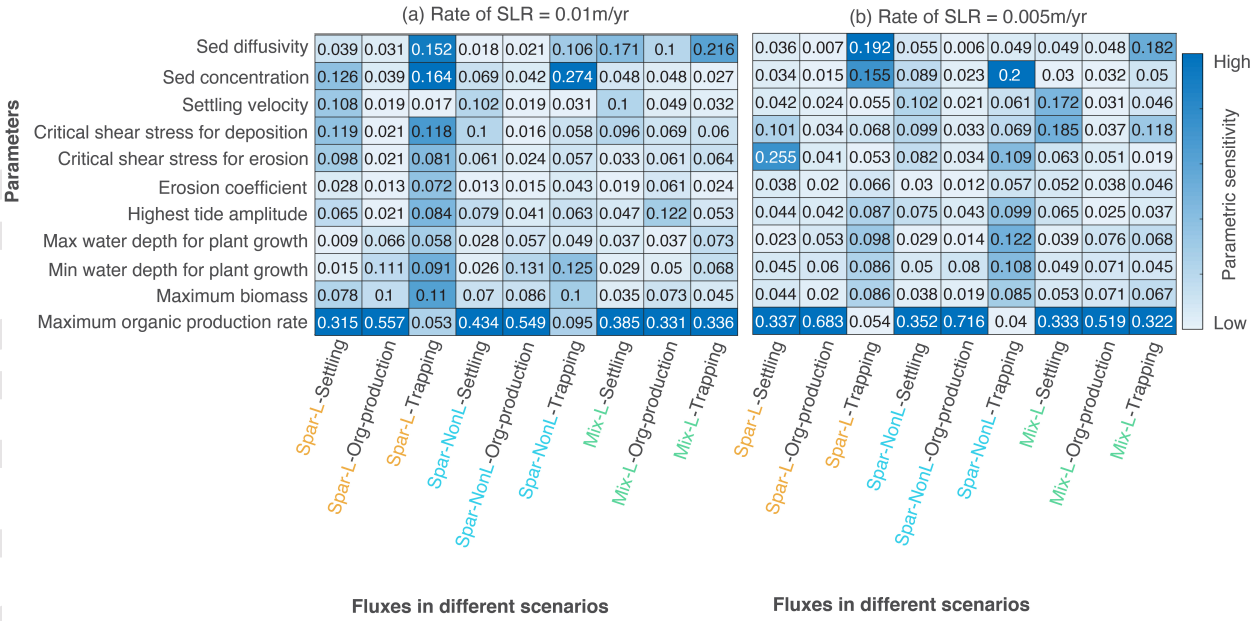

This article is protected by copyright. All rights reserved.

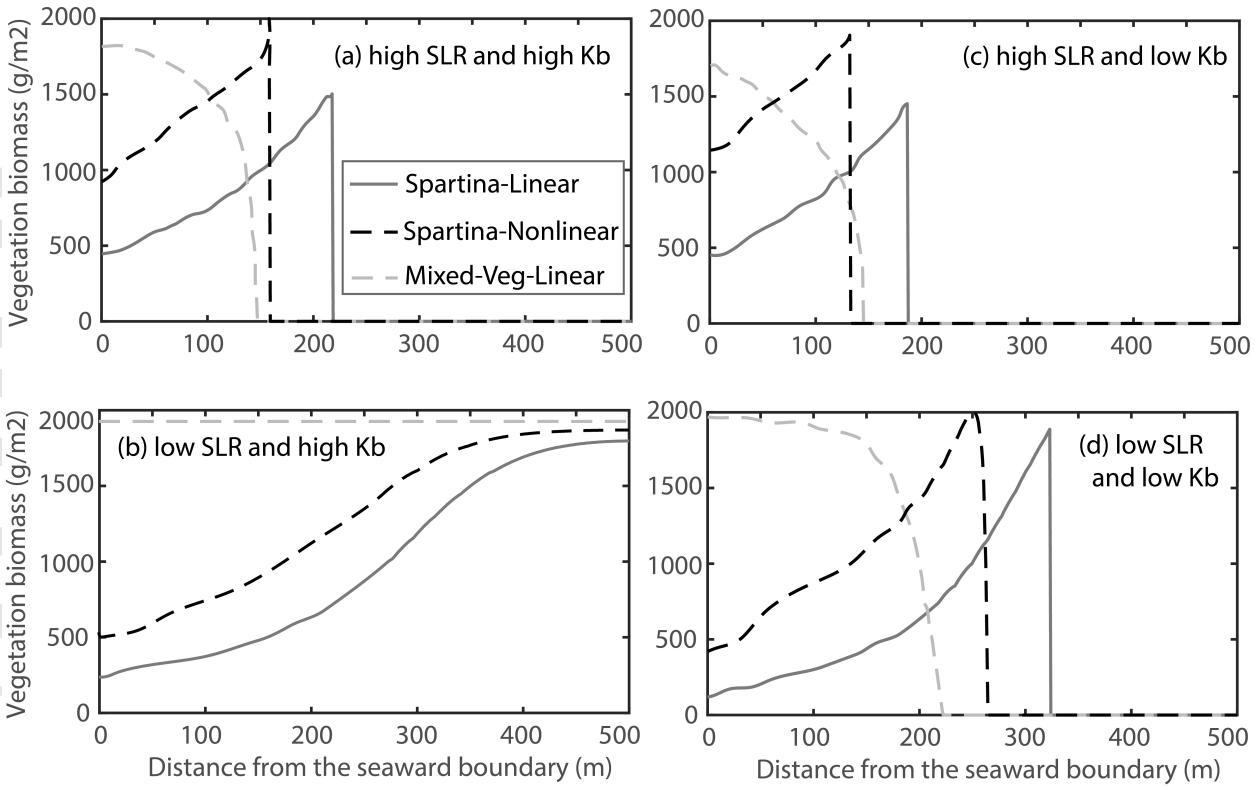

Accepted Article

This article is protected by copyright. All rights reserved.

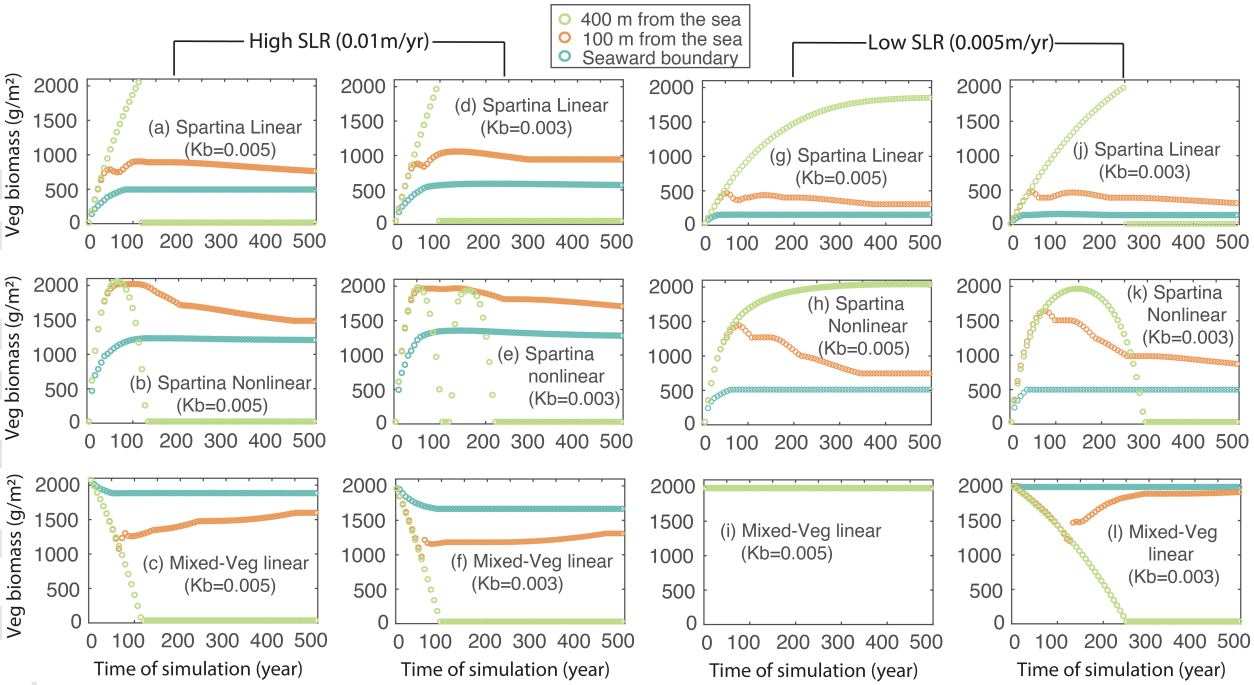

Accepted Article

This article is protected by copyright. All rights reserved.

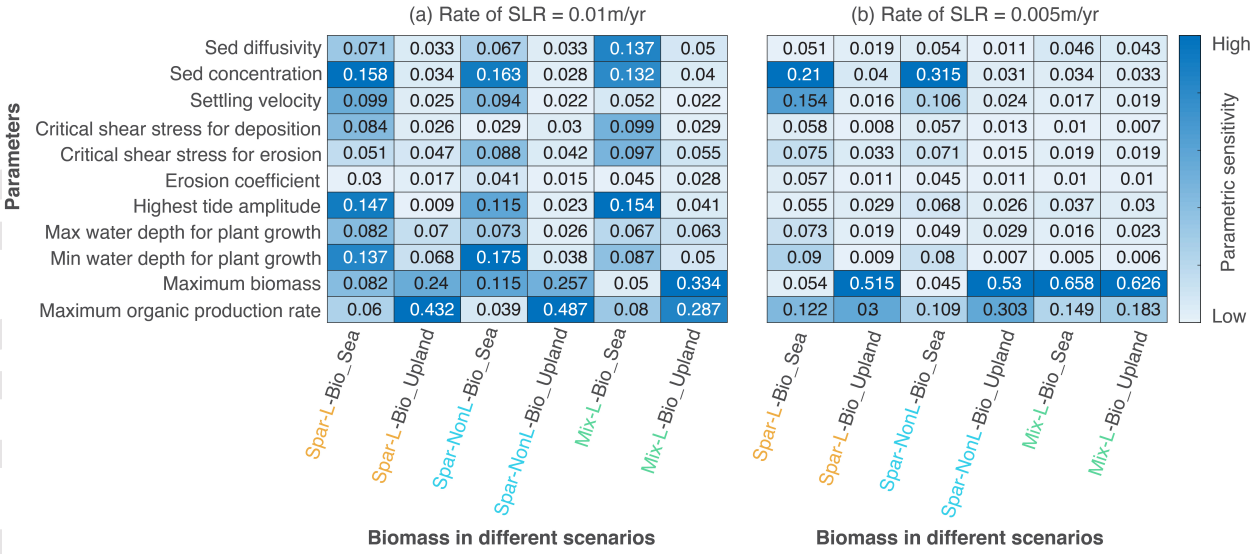

Accepted Article

This article is protected by copyright. All rights reserved.